Photophysical, dynamic and redox behavior of tris(2,6-diisopropylphenyl)phosphine†

René T. Boeré,*[a] Alan M. Bond,*[b] Steve Cronin,[a] Noel W. Duffy,[b] Paul Hazendonk,[a] Jason D. Masuda,[a] Kyle Pollard,[a] Tracey L. Roemmele,[a] Peter Tran[a] and Yuankui Zhang[a]

Received (in Montpellier, France) 27th June 2007, Accepted 14th September 2007
First published as an Advance Article on the web 4th October 2007
DOI: 10.1039/b709602j

The title phosphine, $Dipp_3P$, was synthesized using an aryl copper reagent and the structure determined by X-ray crystallography (R = 2.94%): d(P–C) = 1.852(1) Å, ∠C–P–C = 111.88(5)°. In hexane solution, the electronic spectrum displays 3 bands [326 (9.3), 254 (8.7), 205 (11.4) nm (log|ε|)] and the fluorescence spectrum has a Stokes shift of 129 kJ mol^{-1}. NMR: (δ) ^{31}P = −49.7 ppm in solution and −49.5 in the solid (CP-MAS). Room temperature ^{1}H and ^{13}C spectra reflect D_3 symmetry, changing below −30 °C to C_3. A variable temperature NMR study provided an activation enthalpy of 49(±1) kJ mol^{-1} and entropy of 24–27(±5) J mol^{-1} K^{-1}. An energy surface calculation using HF/3-21G theory discovered a single low-energy path describing pyramidal inversion through a transition state that is close to D_3 geometry. The B3LYP/6-31G(d) calculated barrier to planarization is 37.5 kJ mol^{-1}. Voltammetric studies employing cyclic, rotating disk, steady state and Fourier Transform ac methods confirm a fully chemically reversible one-electron oxidation of $Dipp_3P$ to $Dipp_3P^{+\bullet}$ at +0.18 (CH_3CN–$^{n}Bu_4NPF_6$) and +0.09 (CH_2Cl_2–$^{n}Bu_4NPF_6$) V *vs.* $Fc^{+/0}$ (Fc = ferrocene). The diffusion coefficient for $Dipp_3P$ is 1.0–1.2 × 10^5 cm^2 s^{-1}. The electrode process displays quasi-reversible electron transfer kinetics [$k_s \approx$ 0.01 (CH_2Cl_2) to 0.08 (CH_3CN) cm s^{-1}]. Optically transparent thin layer electrolysis reversibly generates $Dipp_3P^{+\bullet}$ in CH_2Cl_2–$^{n}Bu_4NPF_6$ [UV-Vis: 498 (3.31), 456 (3.29), 373 (4.04), 357 (3.84), 341 (3.49), 296 (3.78), 385 (3.91), 251 (3.99) nm (log|ε|)]. The EPR spectrum of $Dipp_3P^{+\bullet}$ in solution is a doublet (a(P) = 23.9 mT, g = 2.008), and in frozen solution is axial ($a_{\|}$ = 42.6 mT, $g_{\|}$ = 2.0045; $a_{\perp}$ = 12.7 mT, $g_{\perp}$ = 2.0085 mT).

Introduction

Trialkyl- and triarylphosphines[1] are extremely important ligands in organometallic coordination chemistry and many of their characteristics have been systematically categorized by steric bulk ever since the introduction of Tolman's cone angle classification.[2] For many years, the record cone angle of 212° was held by trimesitylphosphine (Mes_3P), **1**.[3,4] Despite its bulkiness, Mes_3P can still form metal complexes, albeit with low coordination numbers, such as in linear Mes_3PAuCl.[5] There is a great deal of current interest in bulky phosphines, both intrinsically and especially in a wide variety of catalytic applications,[6] and recent advances have been reviewed.[6a] The study of phosphorus redox centers has also received considerable attention in recent years,[7] particularly when linked chemically to ferrocene units.[8] Bulky phosphines are also well-known to have restricted intra-molecular dynamics, an old topic which has received renewed attention.[9]

We have been interested for some time in the thermodynamic, kinetic and geometric consequences of high steric bulk. For example, we have designed several ligand systems in which bulky substituents are employed at low-coordinate nitrogen and phosphorus centers.[10] In the course of our work we prepared the new bulky primary phosphine 2,6-diisopropylphenylphosphine ($DippPH_2$) (Dipp = 2,6-diisopropylphenyl; for a full list of abbreviations, see ref. 4).[11] This led us to consider the intriguing possibility as to whether the even more bulky tris Dipp-substituted phosphorus compound could be prepared, and if so what properties it would display.

During the course of our work, the closely-related tris(2,4,6-triisopropylphenyl)phosphine ($Tripp_3P$) was reported by Sasaki, Yoshifuji and co-workers,[12] and several interesting mixed Dipp/Tripp substituent systems in which one ring is substituted at the *para* site have been prepared in order to investigate possible redox interactions.[7f–m] $Dipp_3P$ and $Tripp_3P$ are the most sterically congested triaryl phosphines reported to date.[13]

[a] *University of Lethbridge, Department of Chemistry and Biochemistry, The University of Lethbridge, Lethbridge, AB Canada T1K 3M4. E-mail: boere@uleth.ca; Fax: +1-403-329-2057; Tel: +1-403-329-2045*
[b] *School of Chemistry, Monash University, Clayton, Victoria 3800, Australia. E-mail: Alan.Bond@sci.monash.edu.au; Fax: +61 3 9905 4597; Tel: +61 3 9905 1338*

† Electronic supplementary information (ESI) available: Table S1: Full geometric details. Table S2: Electronic spectra of $Dipp_3P$ and $Dipp_3P^{+\bullet}$ and Ph_3P analogs. Table S3: Calculated hfc constants. Table S4: CV Data. Table S5: Diffusion coefficient values for $Dipp_3P$. Tables S6, S7: Concentration dependence of E_f°. Fig. S1: Static SS ^{31}P NMR spectrum. Fig. S2: Solution ^{1}H NMR of $Dipp_3P$. Figs. S3–5: Eyring plots for DNMR. Fig. S6: Simulated and experimental RDE voltammograms. Fig. S7: Spin density plot of the radical cation. Fig. S8: Walsh diagram for planar and pyramidal EH_3. See DOI: 10.1039/b709602j

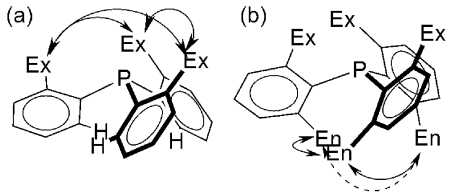

Fig. 1 (a) In a 2-substituted triarylphosphine, the *endo* oriented hydrogen atoms exert mild steric pressure, but the *exo* substituents (Ex) exert reverse steric pressure compressing ∠C–P–C. (b) In a 2,6-disubstituted triarylphosphine, severe steric pressure from the *endo* substituents (En) causes an increase in ∠C–P–C.[12]

Thus, a detailed study of the intrinsic properties of these systems is of particular current relevance.[6a] In a recent conference proceeding, we introduced a distinction between *steric pressure* and *steric shielding* in triaryl phosphines.[14] Thus, a single set of *ortho* substituents (2-position) can provide considerable steric shielding for the phosphorus lone pair, and consequently a large Tolman cone angle, without any flattening of the phosphorus pyramid (Fig. 1(a)). But the presence of substituents in both the 2- and the 6-position of the aromatic ring induces steric pressure which leads to actual flattening of the phosphorus pyramid (Fig. 1(b)).[14] For example, in $(2\text{-}^{i}PrC_6H_4)_3P$, for which the preferred conformation has all the substituents in the *exo* position, $\sum\{\angle CPC\} = 306.5^\circ$, a value which is actually less than in Ph_3P: 308.1°.[15,16] But in $Dipp_3P$ and $Tripp_3P$, the steric pressure generated by the three bulky *endo* substituents causes an increase in $\sum\{\angle CPC\}$ to 335.6 and 334.4°, respectively. A synergistic effect operates such that the flattening caused by the *endo* substituents causes the *exo* substituents to be pushed closer around the phosphorus atom and provides enhanced shielding for the lone pair in these compounds with the same *exo* substituents.[14]

We now report full details of the synthesis, chemical properties, structure as derived from X-ray diffraction and computation, photophysics, solution dynamics and redox behavior of $Dipp_3P$. We demonstrate that it has numerous exceptional properties, which are largely attributable to either steric pressure or steric shielding, but which also involve the inductive influence of the bulky alkyl substituents. The electrochemical investigation employs *inter alia* the new large amplitude form of FT[4] ac-voltammetry which is under development in one of our laboratories.[17]

Whilst there is currently a strong interest in identifying stable and persistent main group element free radicals,[18] there is a paucity of phosphorus-containing examples.[19] Two-coordinate $R_2P^\bullet$ radicals are known, but the only stable derivative is the bis(trimethylsilyl)methyl derivative.[20] A stable diphosphanyl radical $[Mes^*(CH_3)P\text{–}PMes^*]^\bullet$ has also been reported.[21] Stable phosphorus containing radicals that delocalize the unpaired electron over several nitrogen atoms are also known; the 1,3-diphosphaallyl radical $[^{i}Pr_2NP(CN^{i}Pr_2)\text{-}PN^{i}Pr_2]^\bullet$,[22] the tetrakisamidophosphate radicals $\{Li_2[P(N^{t}Bu)_3(NSiMe_3)]LiX \cdot 3THF\}^\bullet$ (X = I, O^{t}Bu),[23] tris(dimethylhydrazino)diphosphine cation,[24] several phosphaverdazyl radicals[25] and a vanadium stabilized NPN radical[26] belong to this category. In contrast, no stable radical cations of triarylphosphines have been reported before this work or that of Sasaki and Yoshifuji,[12] though persistent radicals from sterically congested species such as $Mes_3P^{+\bullet}$, $Duryl_3P^{+\bullet}$ and $Xyl_3P^{+\bullet}$ have been claimed for some considerable time.[27] Last but not least, in order to overcome considerable confusion in the literature, we have measured potentials for the 0/+1 process of several bulky triaryl phosphines under identical conditions in order to put their potentials on a common scale.

Results

Synthesis and properties of $Dipp_3P$

$Dipp_3P$ can be produced in reasonable yield (60–70% of crystalline material) by converting the Grignard reagent prepared from DippBr into $(DippCu)_x$,[28] and reacting *in situ* with PCl_3.[29] There are very few reports on the use of organocopper reagents in the synthesis of triorganophosphines before our work and that of Sasaki and Yoshifuji.[12] Aranyos *et al*. used a biphenylcopper reagent to prepare 2-(di-*tert*-butylphosphino)-biphenyl.[30] Greenfield and Gilbertson used a complex sequence of organozinc followed by lithium cuprate reagents to prepare primary and secondary amino acid derivatives of Ph_2PX.[31] Langer *et al*. have shown the general utility of using organozinc iodides in reactions with Ph_2PCl.[32]

We were unable to measure a melting point for $Dipp_3P$ as it sublimes out of the (capillary) melting point apparatus at atmospheric pressure, reflecting both its high thermal stability and considerable volatility. The radical cation $Dipp_3P^{+\bullet}$ observed in the electron impact mass spectrum also appears to be very stable: the parent molecular ion is not only the base peak in the 70 eV spectrum but is virtually the only ion recorded. The next most abundant fragment (from loss of a single isopropyl group) has a relative intensity of 9%, and two others assigned to $C_6H_{10}P^+$ and $C_7H_7^+$ are each at 4%. Grützmacher and Kirchhoff have discussed the mass spectra of triphenylpnicogens in terms of the element–carbon bond strengths.[33] By way of comparison, in the EI mass spectrum of triphenylphosphine, significant fragments are found for Ph_2P^+ (67%) and PhP^+ (33%) and many other fragments are also produced.[33]

$Dipp_3P$ is remarkably unreactive. It does not appear to react with O_2 from air, even at elevated temperature in solution, nor can the oxide be prepared with H_2O_2 in boiling acetone. Reaction with S_8 in refluxing toluene returned only starting materials, and showed no new ^{31}P NMR peaks, as ascertained by measuring aliquots of the reaction mixture. Similarly, we have not found any metals to which the phosphine coordinates.

Structure from X-ray crystallography

The molecular structure of $Dipp_3P$ as determined by X-ray crystallography is presented in Fig. 2, selected inter-atomic distances and angles in Table 1, and full distances and angles in Table S1, ESI.† All the crystals that we were able to prepare through recrystallization from solvents ranging from alcohols to aliphatic alkanes, as well as by vacuum sublimation, were found to be twinned by merohedry.[34] However, a twin law was found which allowed for successful solution and refinement of the model (R_1 = 2.94%).

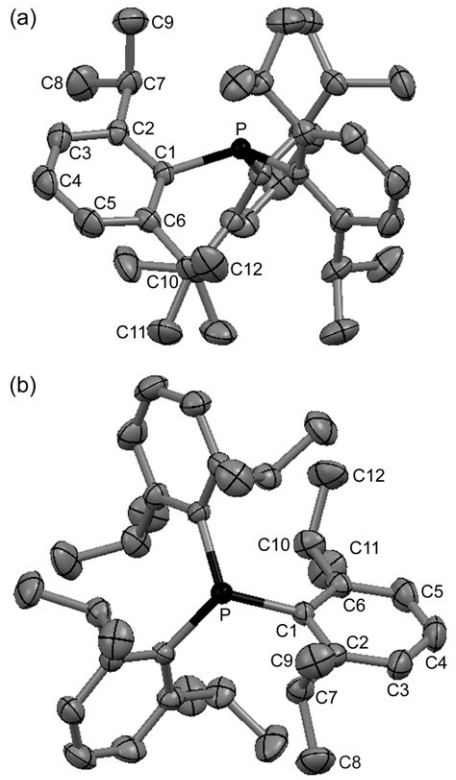

Fig. 2 Thermal ellipsoid diagrams of the $Dipp_3P$ molecule as found in the crystal, (a) viewed down the crystallographic *a* axis and (b) down the *c* axis. The P atom lies on a crystallographic threefold axis and the symmetry-related Dipp rings are generated by the symmetry operations $(-x + y, 1 - x, z)$ and $(1 - y, 1 + x - y, z)$. H atoms are omitted for clarity. Space-filling diagrams of these two views are available in the preliminary communication.[14]

The converged model from the crystallographic study shows the typical ''propeller'' configuration of triaryl phosphines, with the three aryl rings tilted to minimize interatomic repulsion. The molecular three-fold rotation axis aligns with the crystallographic three-fold axis of the triclinic space group *R*3, rendering the geometry of each of the Dipp groups identical. The P–C bond length is 1.851(2) Å, the C–P–C bond angle is 111.88(5)°, and the sum of angles around phosphorus, $\sum\{\angle CPC\}$, is 335.64°. Each of these parameters is slightly greater than those reported for $Tripp_3P$ (P–C range from 1.839–1.851 Å; ∠CPC range from 110.9(1)–111.9(1)°;[12] $\sum\{\angle CPC\}$ = 334.41°),[14] which crystallizes without crystallographic site symmetry in $P\bar{1}$. The slightly greater flattening in $Dipp_3P$ *vs.* $Tripp_3P$ is also substantiated by HF/6-31G(d) calculations ($\sum\{\angle CPC\}$ = 337.01 and 336.80°, respectively).[14] The P atom is found to be 0.43 Å out of the least squares plane defined by C2, 3, 5, 6, which is more than in less congested $DippPR_2$ moieties, such as $DippP(H)Si^tBuMe_2$, where the P is only 0.32 Å out of the aromatic carbon atom plane.[11]

Fluorescence spectrum

Triphenylphosphine shows an unusually large fluorescence Stokes shift, which has been attributed to the occurrence of a large geometrical change from pyramidal in the ground state to near planar in the excited state.[35] We therefore measured the UV-Vis and fluorescence spectra of $Dipp_3P$ in anticipation of observing a smaller Stokes shift because of its flattened ground state structure. The spectra (Table S2, ESI,† Fig. 3) indeed demonstrate a much smaller Stokes shift in hexanes of 129 kJ mol^{-1} compared to 201 kJ mol^{-1} for Ph_3P.

NMR studies

Solution ^{31}P NMR. The ^{31}P chemical shift of $Dipp_3P$ in solution in $CDCl_3$ is found at a high frequency for a triarylphosphine, −49.7 ppm. For comparison, the shifts are −6 in Ph_3P, −35.3 in Xyl_3P, −37.2 in Mes_3P, −29.7 in $Duryl_3P$ and −53 ppm in the isosteric $Tripp_3P$.[12,36] It has been shown that ∠C–P–C angles are major contributors to the chemical shifts of triorganophosphines, but larger angles are usually associated with low-frequency chemical shifts.[37] The comparison with $Tripp_3P$ indicates that the inductive electronic effect of the isopropyl substituents on the phosphorus shielding tensor is not negligible.

Solid state (SS ^{4}) ^{31}P NMR. The purpose in recording the solid-state ^{31}P NMR spectrum was to look for possible magnetic inequivalence associated with twinning in the crystals. The static solid-state ^{31}P spectrum of $Dipp_3P$ obtained with direct polarization and proton decoupling has $\Delta\nu_{1/2}$ = 4.4 kHz, while the 15 kHz MAS spectrum under the same conditions is a narrower singlet with $\Delta\nu_{1/2}$ = 170 Hz and a chemical shift of −49.5 ppm with respect to external 85%

Table 1 Selected interatomic distances (Å) and angles (°) for $Dipp_3P$ and $Dipp_3P^+$ from X-ray diffraction and computation[a]

	X-Ray diffr. $Dipp_3P$	C_3 in B3LYP/ 6-31G(d)	D_3 in B3LYP/ 6-31G(d)	C_3 in HF/ 6-31G(d)	$[Dipp_3P]^+$ in UHF/ 6-31G(d)
P–C1	1.8507(16)	1.8781	1.8142	1.8777	1.8353
C1–C6	1.418(2)	1.4236	1.4272	1.4122	1.4164
C1–C2	1.425(2)	1.4310		1.4221	1.4187
P oop of C1 × 3[b]	0.539	0.536	0	0.531	0.193
P oop C2–C3–C5–C6[c]	0.430	0.434	0	0.424	0.060
C1#1–P–C1	111.88(5)	112.2	120.0	112.3	118.9
C6–C1–C2	118.90(16)	118.8	121.4	118.5	121.3
C6–C1–P	127.17(13)	126.8		127.2	122.5
C2–C1–P	113.10(12)	113.4	119.3	113.4	116.2

[a] Symmetry transformation used to generate equivalent atoms: #1 $(-x + y, 1-x, z)$. [b] Out of the plane of the three *ipso* C atoms of the aryl rings. [c] Out of the plane of the four *ortho* and *meta* C atoms of the aryl ring.

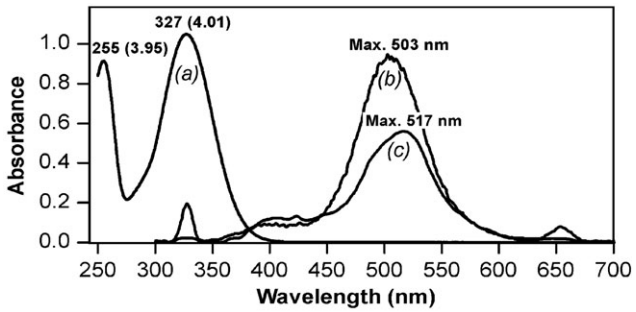

Fig. 3 (a) Electronic absorption spectrum in hexanes (λ_{max} in nm; log|ε| in parentheses) and fluorescence spectra of $Dipp_3P$ in hexanes (b) and ethanol (c). The fluorescence intensity scale is arbitrary.

H_3PO_4. Cross-polarization (CP ^{4}) results in very similar spectra (Fig. S1, ESI†). The static SS ^{31}P NMR spectrum under CP conditions of $Tripp_3P$ has been reported without details.[6a]

Solution ^{1}H and ^{13}C NMR. The NMR parameters (see Table 2) of the compound substantiate the putative molecular structure, but are indicative of dynamic effects because the RT ^{1}H and ^{13}C NMR spectra (in both $CDCl_3$ and CD_2Cl_2 solutions) reflect unexpectedly high molecular symmetry (*i.e.* D_3, Fig. S2, ESI†). The *para* and *meta* aromatic proton signals are distinctly resolved (as commonly seen in Dipp chemistry), forming a *pseudo*triplet and *pseudo*doublet, but the latter is further split by coupling to ^{31}P. The isopropyl CH resonance is found at 3.497 ppm and is a doublet of septets from coupling to phosphorus and to the methyl protons. There are two distinct isopropyl methyl resonances, one at 1.17 ppm, the other at 0.71 ppm, and this latter is appreciably line broadened at RT in both the 250 and 500 MHz spectra. This last resonance is somewhat deshielded from the natural resonance position of such methyl groups, which, based on the X-ray and *ab initio* structure determinations and much previous experience, we attribute to the "paraphane" effect, *i.e.* anisotropic shielding induced when the protons on a methyl group are swept across the surface of a neighbouring aromatic ring.[10] In the ^{13}C spectrum, two methyl carbon resonances (with the lower field signal dynamically broadened), one methine and four from the benzene ring are observed at RT.

On cooling dilute solutions in either $CDCl_3$ or (better) CD_2Cl_2, the ^{1}H and ^{13}C resonances go through smooth coalescences and sharpen considerably by −80 °C, at which point general line broadening limits further improvements in the appearance of the spectra; fortunately at this temperature the spectra are very clear. A low-temperature COSY spectrum was measured to confirm the assignment of the ^{1}H NMR signals (−60 °C). The LT spectra of both nuclei define a static structure in which the rotation of the isopropyl substituents is frozen out and only methyl group rotation is fast on the NMR timescale, and thus is consistent with molecular C_3 symmetry (Fig. S2, ESI†). There are in all four methyl and two methine carbon environments. There are six different ^{13}C resonances in the benzene ring. Most significantly, the coupling to ^{31}P observed in the RT ^{13}C spectra are found in each case to become localized on nuclei belonging to one half of the Dipp group at LT, consistent with conjugation to phosphorus in one orientation, or of through-space interaction with the phosphorus lone pair. These couplings are typically about twice as large at those observed in the averaged signals at RT.

Dynamic NMR measurements. A thorough dynamic NMR investigation of $Dipp_3P$ using both ^{1}H and ^{13}C spectra was undertaken. The barriers for the DNMR processes were determined using two methods, line shape analysis (LSA) and the full width at half height method ($\Delta\nu_{1/2}$).[38] The analyses were undertaken by complete line fitting for the methyl regions in the ^{1}H (Fig. 4) and ^{13}C (Fig. 5) spectra where the rate and $\Delta\nu_{1/2}$ were determined as a function of temperature. The rates were related to temperature using the Eyring relationship, where $\ln(k/T)$ was plotted as a function of $1000/T$ (Fig. S3–5, ESI†) to determine the activation enthalpy, $\Delta H^{\ddagger}$, from the slope and the activation entropy, $\Delta S^{\ddagger}$, from the intercept. (Merely using the temperature dependence of $\Delta\nu_{1/2}$, only an upper bound to $\Delta H^{\ddagger}$ can be obtained from the slope of an "Eyring like" plot of $1/\Delta\nu_{1/2}T$ *vs.* $1/T$; however all information on $\Delta S^{\ddagger}$ is lost.) This analysis is specific to uncoupled equally populated AB systems, where the temperature dependence of the frequency difference between A and B is expected to be weak, as is the case for carbon and less so for proton. Table 3 lists the energetic results of the analysis, and the original plots are provided in the ESI.†

Table 2 ^{1}H and ^{13}C NMR data for $Dipp_3P$ at ambient and low temperature[a]

	C_1	C_2	C_6	C_4	C_3	C_5	C_{10}	C_7	C_9	C_{11}	C_8	C_{12}
^{1}H: +30 °C, CD_2Cl_2												
δ	—	—	—	7.288	7.105		3.497		1.173		0.709	
J_{HH}/Hz	—	—	—	7.68	7.68		6.72		6.72		6.72	
J_{HP}/Hz	—	—	—	0	3.28		5.20		0		0	
^{1}H: −80 °C, CD_2Cl_2												
δ	—	—	—	7.27	7.07	7.07	3.30	3.14	1.13	0.99	0.90	0.36
J_{HH}/Hz	—	—	—	7.76	7.58	7.58	~6	~6	6.1	6.3	6.3	6.2
J_{HP}/Hz	—	—	—	0	3.3	3.3	0	~6.4	0	0	0	0
^{13}C: +20 °C, $CDCl_3$												
δ	135.37	153.64		129.38	124.37		32.37	32.37	23.30		24.82	
J_{CP}/Hz	25.9	18.6		0	3.9		17.6	17.6	0		0	
^{13}C: −80 °C, CD_2Cl_2												
δ	134.26	153.00	151.94	128.64	125	122.47	32.19	31.40	21.77	22.65	23.59	24.41
J_{CP}/Hz	25	40	0	0	6	0	0	32	0	0	0	0

[a] The atom numbering scheme is that used in Fig. 2; H atoms are those attached to the labeled C.

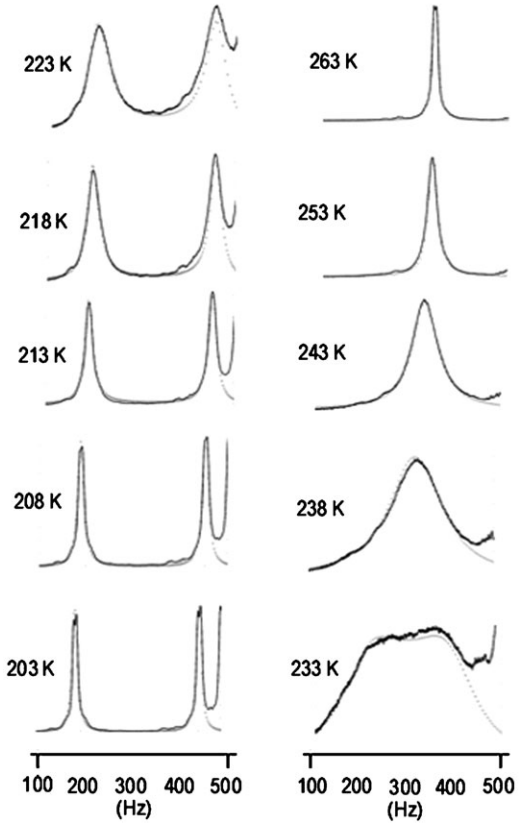

Fig. 4 Line-shape fitting for the isopropyl methyl group signals of the ^{1}H NMR spectra of $Dipp_3P$ as employed in line shape analysis. The gray lines represent the fits to the experimental data.

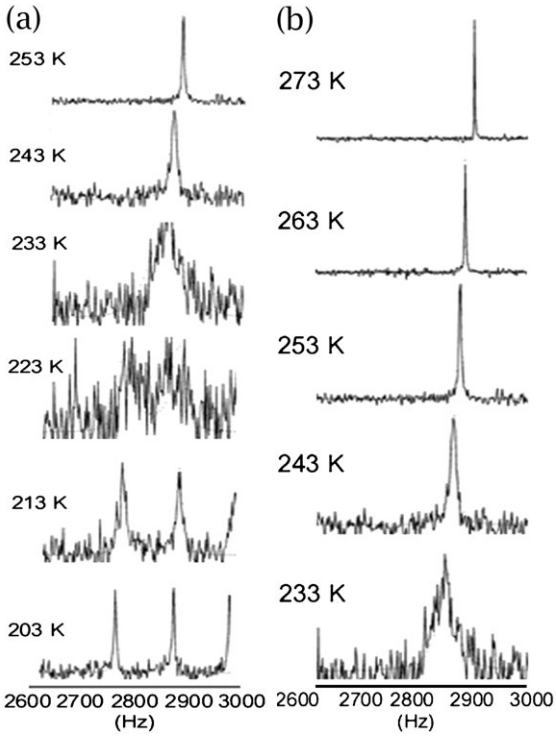

Fig. 5 Line-shape fitting for the isopropyl methyl group signals of the ^{13}C NMR spectra of $Dipp_3P$ as employed in (a) Line shape analysis (LSA) and (b) full-width at half-height ($\Delta\nu_{1/2}$) analysis. The gray lines represent the fits to the experimental data.

The values obtained for the enthalpy of activation of the dynamic process measured from the different signals are reasonably coherent. The results from the proton LSA indicate that the enthalpy lies near 49 ± 1 kJ mol^{-1}, but this value is greatly underestimated by the $\Delta\nu_{1/2}$ method, especially when using ^{1}H NMR data. The lineshape analysis method was augmented with data from selective inversion experiments at the lowest four temperatures, which serves to correct for systematic errors commonly encountered when relying on LSA alone. This results in more accurate results but often with higher statistical uncertainty.[39] The carbon analyses agree well within experimental error with the LSA proton results. A free energy of activation for $Tripp_3P$ has been reported as 46.0 kJ mol^{-1} at 243 K (in excellent agreement with our results), which was also attributed to an inversion process, but no details of the analysis are provided.[6a] The LSA on ^{1}H spectra indicates that the entropy of activation is positive with a value of 24–27(±5) J mol^{-1} K^{-1}. The large positive activation entropy indicates an increase in the molar volume when going to the transition state. It also indicates that the solvent rearranges to a less ordered state when the molecule is promoted from the ground to the transition state.

Quantum chemical calculations

We have obtained the structure of $Dipp_3P$ in the C_3 ground and D_3 transition states by both HF/6-31G(d) and B3LYP/6-31G(d) methods and $[Dipp_3P]^{+\bullet}$ at the UHF/6-31G(d) level of theory only. Our attempts to optimize the structure of the latter by DFT were not successful, but UB3LYP/6-31G(d)//UHF/6-31G(d) calculations were performed at the HF optimized geometry to determine the hyper-fine coupling constants (Table S3, Fig. S7, ESI†). The geometrical results (Fig. 6) are presented in Tables 1 and S1, ESI,† and show the very close agreement between the X-ray crystal and ground-state calculated structures determined for $Dipp_3P$ at the two levels of theory. The only significant deviation is in the C–P bond lengths, which are longer in the calculated compared to the experimental structure of the neutral molecule. Note that the *experimental* C–P bond distance at 1.851(2) is itself significantly longer than the average value of 1.836(10) Å determined for 102 triaryl phosphines reported in the CCDC database.[40] The calculations also accurately reproduce the distortion of the P atom out of the plane of four carbon atoms of the aromatic rings (the two *ortho* and two *meta* atoms are used to define these planes, see above). Another measure of a pyramidal geometry is the deviation of the P atom from the plane defined by the three *ipso* carbon atoms of the Dipp rings. Here too there is excellent agreement between the diffraction results and the two computational methods.

An estimate of the energy of a possible planar transition state structure of $Dipp_3P$ has been calculated by constraining the molecule to D_3 symmetry (Fig. 6(b)). The energy difference between the C_3 ground state and this planar geometry is 37.5 kJ mol^{-1}, implying a very low gas-phase barrier to pyramidal inversion at the B3LYP/6-31G(d) level of theory. This planar structure has P–C bonds that are 0.064 Å shorter than in the

Table 3 Energetic data from DNMR measurements for $Dipp_3P$

	Proton		Carbon		Method
	Methyl downfield	Methyl upfield	Methyl upfield	Methyl downfield	
Slope (from $\Delta\nu_{1/2}$ plots)	-4.92 ± 0.18	-5.01 ± 0.19	-5.41 ± 0.08	-5.58 ± 0.18	$\Delta\nu_{\frac{1}{2}}$
Enthalpy/kJ mol^{-1}	40.9 ± 1.5	41.7 ± 1.6	45.0 ± 0.7	46.4 ± 1.5	
Slope (from Eyring plots)	-5.89 ± 0.09	-5.94 ± 0.09	-6.35 ± 0.36	-6.13 ± 0.47	LSA
Enthalpy/kJ mol^{-1}	48.98 ± 0.69	49.39 ± 0.71	52.80 ± 3.0	50.99 ± 3.9	
Entropy/J mol^{-1} K^{-1}	24.8 ± 4.3	27.0 ± 4.5	44.0 ± 19.7	34.7 ± 25.1	

ground state, suggesting that the steric congestion of the bulky Dipp groups is relaxed significantly when the phosphorus lone-pair becomes stereochemically inactive.

The structure of $Dipp_3P^{+\bullet}$ at the UHF/6-31G(d) level of theory is almost, but not entirely, planar at phosphorus, with $\angle$C–P–C = 118.9° and a deviation of the P atom out of the plane of the *ipso* carbon atoms of only 0.193 Å (Fig. 6(d)). The distortion of the P atom out of the plane of four carbon atoms of the aryl ring is also greatly relieved at only 0.060 Å. Thus the single remaining non-bonded electron at phosphorus has lost almost all of its stereochemical activity; this will have important consequences for the EPR spectrum of the radical cation (see below). In this species, the P–C bonds are also considerably shorter than those in the neutral analog—whether by comparison to the X-ray structure or to the HF/6-31G(d) calculations—which is also indicative of the relaxation of steric pressure in the ion.

Electrochemistry

Cyclic voltammetry

$Dipp_3P$ undergoes an initial chemically reversible oxidation process (Fig. 7) at modest potentials (slightly more positive than for oxidation of Fc) on Au, Pt and GC electrodes in both CH_3CN and CH_2Cl_2 solvents (see Table 4 and S4, ESI†). Comparison of characteristics such as larger peak-to-peak separation, relative to that of known reversible one-electron $Cc^{+/0}$ and $Fc^{+/0}$ processes measured under the same conditions, implies that a quasi-reversible one-electron process:

$$Dipp_3P \rightleftharpoons [Dipp_3P]^{+\bullet} + e^- \quad (1)$$

is detected under conditions of cyclic voltammetry. Additionally, the presence of a small level of uncompensated resistance in the form of Ohmic iR_u is indicated from the concentration dependence in CH_2Cl_2. A second, irreversible, oxidation process labeled as B in Fig. 7 is observed at a considerably more positive potential just prior to the solvent limit in CH_2Cl_2. Whether this is derived from further oxidation to P(v), or an oxidation at the electron-rich aryl ring, has not yet been elucidated and this process is not discussed further. The almost linear plots of the I_p *vs.* $\nu^{1/2}$ obtained for the first $Dipp_3P$ oxidation process in CH_3CN and CH_2Cl_2 at GCE, Pt and Au working electrodes imply that the mass transport process at the peak potential is controlled by diffusion. From the Randles–Sevcik relationship:[41]

$$I_p = kn^{2/3}AD^{1/2}C\nu^{1/2} \quad (2)$$

an estimation of the diffusion coefficient was obtained from a straight line fit to the I_p *vs.* $\nu^{1/2}$ plots. Results are summarized

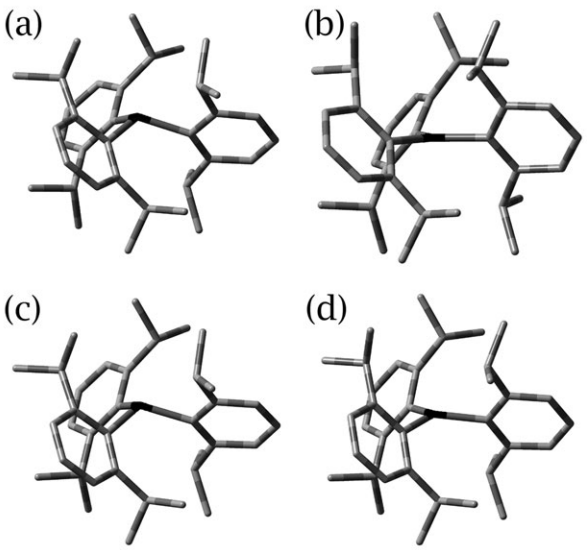

Fig. 6 B3LYP/6-31G(d) computed structures of (a) $Dipp_3P$ in the C_3 ground state and (b) D_3 planar transition state. (c) HF/6-31G(d) computed structure of $Dipp_3P$ and (d) UHF/6-31G(d) computed structure of $Dipp_3P^{+\bullet}$. The "tube" representations show only the P (black) and C (gray) atoms.

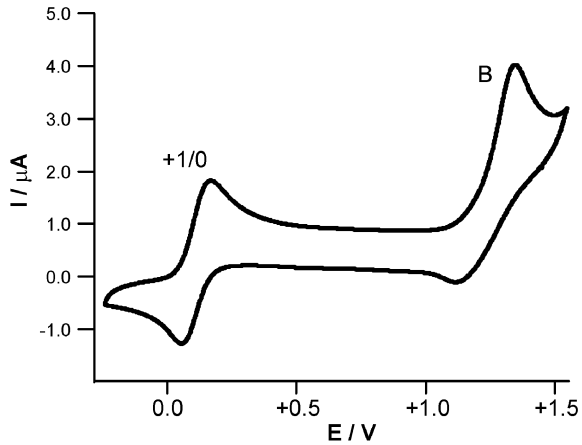

Fig. 7 Cyclic voltammetry of $Dipp_3P$ (0.20 mM) in CH_2Cl_2 solution containing 0.4 M $^nBu_4NPF_6$ under an atmosphere of dry N_2 recorded at scan rate of 200 mV s^{-1} using an Au macrodisk electrode at 0 °C. Potentials *vs.* $Fc^{+/0}$. Note the wide window within which $[Dipp_3P]^{+\bullet}$ is stable; the secondary process labeled "B" has not been investigated in detail.

Table 4 Reversible potentials (V)[a] obtained for the $[Dipp_3P]^{+/0}$ process

Solvent	CH_2Cl_2[b]	CH_3CN[b]
E_f° *vs.* $Fc^{+/0}$	0.09[c]	0.18[c]
E_f° *vs.* $Cc^{+/0}$	1.44	1.53
E_f° *vs.* $Fc^{*+/0}$	0.66	0.70
ΔE_f° ($Cc^{+/0}$ − $Fc^{*+/0}$)	0.79	0.84
E_a (2nd process) *vs.* $Fc^{+/0}$	1.25[d]	

[a] Calculated by cyclic voltammetry from the average of oxidation and reduction peak potentials. [b] Containing 0.1 M $^nBu_4NPF_6$ at 295 K. [c] $Cc^{+/0}$ data converted to the $Fc^{+/0}$ scale by subtraction of 1.35 V. [d] Scan rate = 0.2 V s^{-1}.

in Table S5, ESI.† Excellent agreement was obtained between digital simulation and experimental results for a quasi-reversible one-electron oxidation using the parameters given in Table 5 (Fig. 8). The estimate of the diffusion coefficient from simulation was in agreement with the values obtained independently from steady state methods on micro-Pt and -carbon electrodes and hydrodynamic measurements at a rotating disc electrode (Table S5, ESI†).

Since the structure of $Dipp_3P$ is close to spherical, and presents a sheath of hydrocarbon to the surrounding environment, specific solvation interactions are expected to be minimal. The similar electrochemical behavior in CH_3CN and CH_2Cl_2 can be rationalized on this basis, despite the fact that these solvents are at opposite ends of the dielectric constant scale. This also implies that the Stokes–Einstein equation, which relates the radii and diffusion coefficients of molecules, ought to be approximately valid. Measurements of the distances between H nuclei at opposite ends of the molecule, and adding 1.20 Å to each H for the van der Waals radius, gives a diameter perpendicular to the three-fold axis of 12.6 Å and parallel to the axis of 10.7 Å, thereby describing a slightly oblate spheroid with a dimensional ratio of 0.85. On the reasonable assumption that the molecule is approximately spherical, a simple average radius can be taken as 5.8 Å. Hence the diffusion coefficient can be calculated from the Stokes–Einstein equation:[42]

$$D_i = k_B T/6\pi\eta r \quad (3)$$

where k_B is the Boltzman constant, T the absolute temperature, η the (normal) viscosity of the solution and r the radius of the dissolved molecule. On the reasonable assumption that the viscosity of a CH_3CN (0.1 M $^nBu_4NPF_6$) solution is close to that of the pure solvent (0.369 mN s m^{-2} at 20 °C),[43] we get a

Table 5 Parameters obtained from digital simulation of a cyclic voltammogram of $Dipp_3P$[a]

Solvent	Electrode	$10^{-5}D$/cm^2 s^{-1}	α	k_s/cm^2 s^{-1}	$R_{measured}$/Ω
CH_3CN	Pt	1.25	0.5	0.04	330
	GC	1.00	0.5	0.08	180
CH_2Cl_2	Pt[b]	1.10	0.5	0.01	3100
	GC	1.20	0.5	0.01	1400

[a] Determined by comparison of experimental data and simulated cyclic voltammograms. [b] With 0.05 M $^nBu_4NPF_6$ supporting electrolyte; all other data obtained with 0.1 M $^nBu_4NPF_6$.

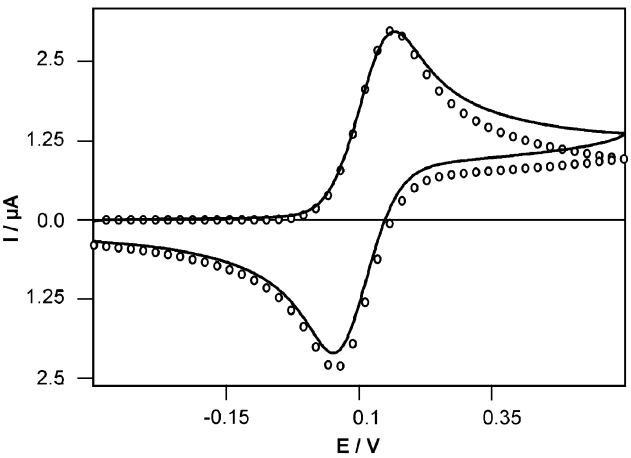

Fig. 8 Comparison of cyclic voltammograms obtained for oxidation of $Dipp_3P$ (0.56 mM) at a scan rate of 100 mV s^{-1} at a 1.6 mm Pt disk electrode in CH_2Cl_2 (0.05 M $^nBu_4PF_6$) (—) and by simulation using parameters provided in Table 5 (○).

value at 295 K for $D_i = 1.0 \times 10^{-5}$ cm^2 s^{-1}. This value is in good agreement with the values for D measured for dilute solutions of $Dipp_3P$ in CH_3CN by RDE and steady-state voltammetry. D for $Mes_3P^{+/0}$ has been estimated in CH_3CN to be $D = 1.6 \times 10^{-5}$ cm^2 s^{-1}.[44]

It is difficult to compare potentials obtained in different solvents. However, assuming that the reversible potential for the $Cc^{+/0}$ process is independent of solvent, then there is a difference of about 90 mV in the E_f° of the $[Dipp_3P]^{+/0}$ process with respect to the $Cc^{+/0}$ redox couple in changing from CH_2Cl_2 to CH_3CN (Table 4). If Cp^*_2Fe is used as an internal standard and the value assumed to be solvent independent, then a smaller shift of about 60 mV is observed.[45] Bond *et al.* have shown that the difference between E_f° ($Fc^{+/0}$) and E_f° ($Cc^{+/0}$) is solvent independent ($\Delta E_f^\circ = 1.35 \pm 0.01$ V), but this does not confirm that each couple is independent of solvent.[46] The observed solvent dependence could be due to the reference scale independent approximation or differences in ion pairing between $[Dipp_3P]^{+\bullet}$ and electrolyte in the two solvents or a small level of solvent interaction. A study where the ionic strength was varied significantly from 0.05 to 0.50 M (Table S6, ESI†) as was the concentration of $Dipp_3P$ (0.5 to 2.8 mM) induced a range of reversible potentials of only 20 mV. Thus, neither ion-pairing nor solvent effects are considered to be large contributors to the reversible $[Dipp_3P]^{+/0}$ potentials.

Broadening of the voltammetric wave shape and peak potential shifts with increasing analyte concentrations are typically assigned to the influence of uncompensated resistance in CH_2Cl_2 containing 0.05 to 0.5 M $^nBu_4NPF_6$. However, a close to linear scaling of the Faradaic current is observed (Table S7, ESI†) with concentration of analyte in CH_2Cl_2 (0.5–5.0 mM) which implies that the influence of uncompensated resistance on the voltammograms is minimal under these high supporting electrolyte conditions. Furthermore, the linear dependence of I_p *vs.* concentration of $Dipp_3P$ at constant scan rate provides an estimate of the diffusion coefficient (1.04×10^{-5} cm^2 s^{-1}) from the slope and Randles-Sevcik

relationship which is in excellent agreement with the other determinations reported in Table S5, ESI.†

Fourier transform voltammetry

The significant advantages of employing large amplitude ac voltammetry in conjunction with Fourier reconstructions for the analysis of electrode processes have been recently demonstrated.[17] In a typical dc voltammetric experiment, it is not necessarily obvious which terms (*e.g.* uncompensated resistance, capacitance, k_S, E_f°, α) determine the shape and other characteristics of the observed voltammograms. With the large amplitude ac method and access to data over a wide frequency range in a single experiment, the dc term is retained, but numerous additional easily identifiable patterns of behavior are now available from the power spectrum and the fundamental, second, third and higher harmonics. Each of these terms exhibit characteristic dependencies on the above parameters that depend on concentration, frequency and scan rate, but with different levels of sensitivity, so that the prospect of obtaining a unique solution to the electrode mechanism is greatly enhanced.

Fig. 9 illustrates the data collected in a large amplitude ac voltammetric experiment, displayed as a function of time. Deconvolution into the dc component and ac harmonics (Fig. 10) is achieved by a Fast Fourier Transform (FFT)–Inverse Fast Fourier Transform (IFFT) sequence.[17f] The patterns displayed in the harmonics presented in Fig. 10 are fully consistent with both a quasi-reversible electron-transfer process and uncompensated resistance. Importantly, increasing the concentration of $Dipp_3P$ from 0.50 mM up to 9.23 mM leads to very characteristic changes in the third and higher harmonics that can be well modeled by incorporating both slow electron kinetics and uncompensated resistance. These patterns cannot be simulated by considering uncompensated resistance effects or slow electron transfer alone.

Spectroelectrochemistry

Optically transparent thin-layer electrolysis (OTTLE) spectroscopic[47] monitoring of the oxidation of $Dipp_3P$ was conducted on a 1.01×10^{-3} M solution of $Dipp_3P$ in CH_2Cl_2 containing 0.1 M $^nBu_4NPF_6$, which was protected from the atmosphere by a blanket of N_2 gas. An initial recording of the electronic spectrum was undertaken before electrolysis (Fig. 11). During oxidative electrolysis, continuous repetitive spectral scans from 800 to 250 nm were recorded until such time that the current was 1% of the initial value. Fig. 11 also presents key spectra selected from the 38 recorded during forward electrolysis. The many isosbestic points are consistent with the direct conversion of species $Dipp_3P$ to $[Dipp_3P]^{+\bullet}$. Furthermore, the resulting solution of oxidized material was subsequently reduced at an applied potential held 0.4 V more negative than the oxidation, resulting in almost complete conversion of the spectroscopic signal back to that of $Dipp_3P$.

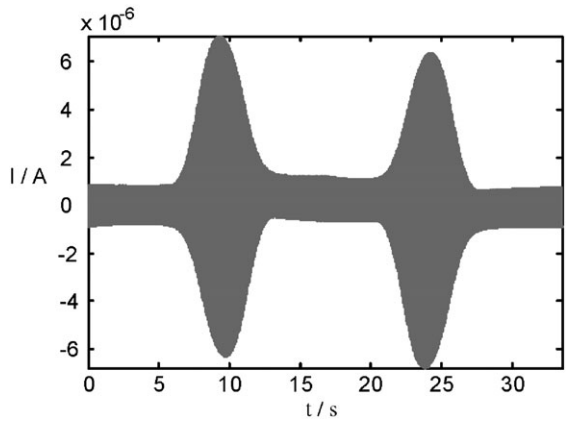

Fig. 9 *I–t* data obtained from a large amplitude ac voltammogram of $Dipp_3P$ (0.5 mM) in CH_2Cl_2 (0.51 M $^nBu_4NPF_6$) solution at a 0.94 mm diameter Pt disk electrode; ν = 47.68 mV s^{-1}, freq. = 21.46 Hz, amp = 80 mV. Data obtained over the potential range of 0–1 V *vs.* $Ag^{+/0}$, 65 536 data points collected.

The final scan in Fig. 11 represents the best-characterized UV-visible spectrum of a triarylphosphine radical cation. The spectrum of $Dipp_3P^{+\bullet}$ is extremely rich (data in Table S2), consisting of (at least) two broad bands in the visible region (λ_{max}: 498 and 456 nm), and several sharp bands in the UV region (λ_{max}: 373, 357, 341(sh), 296(sh), 285, 281(sh), 251 nm). In this spectral region in CH_2Cl_2, $Dipp_3P$ only has two bands (λ_{max}: 327 and 255 nm). Previously, only poorly resolved spectra of $Ar_3P^{+\bullet}$ were known, produced in various matrices by pulse radiolysis. These spectra show broad, ill-defined features with lowest energy maxima of *ca.* ~500–530 nm.[48] The qualitative appearance of the spectra reported for $Ph_3P^{+\bullet}$ and $(p\text{-Tol})_3P^{+\bullet}$ at 77 K in *n*-butyl chloride matrices, however, are in agreement with our results.[49] It seems likely that the rich spectral features of the radical cation reflect transitions between the remaining phosphorus non-bonded electron and the many π* levels of the electron rich Dipp aryl rings. The visible bands account for the distinct orange color of dilute solutions of $Dipp_3P^{+\bullet}$ salts. $Ph_3N^{+\bullet}$ has an intense absorption at 640 nm attributed to delocalization of the unpaired electron over the aryl rings.[50] The absence of such a very-low energy band, as well as evidence from EPR spectra (see below), is against the hypothesis of extensive delocalization of this kind in $Dipp_3P^{+\bullet}$.

Bulk electrolysis

The course of oxidative bulk electrolysis of $Dipp_3P$ in CH_2Cl_2 (0.1 M $^nBu_4NPF_6$ at 200 mV positive of E_f°) at a Pt gauze basket electrode was monitored by obtaining rotating disk electrode (RDE) voltammograms before and after exhaustive oxidative electrolysis (Fig. 12 and S6, ESI†). The identical magnitude, but opposite sign of the limiting currents confirms that $Dipp_3P$ is quantitatively oxidized to $[Dipp_3P]^{+\bullet}$. Quantitative conversion back to $Dipp_3P$ was also achieved. Coulometric measurements confirm that the oxidation process and reduction back to starting material both involve the transfer of one electron (n = 0.88) per molecule. The radical cation $[Dipp_3P]^{+\bullet}$ produced was shown to be stable for at least 2 h when generated by bulk electrolysis.

EPR spectra

Samples of $[Dipp_3P]^{+\bullet}$ were first obtained by bulk electrolysis in CH_2Cl_2 (0.1 M $^nBu_4NPF_6$). In one case, the solution at the end of exhaustive electrolysis was transferred, with full

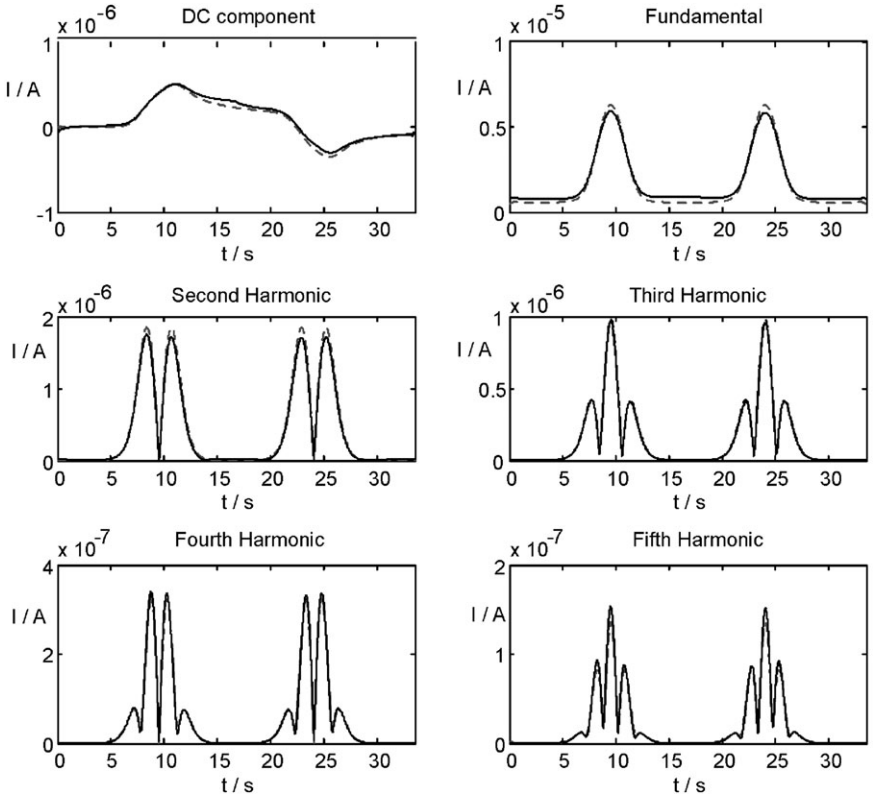

Fig. 10 DC, fundamental and first four harmonic components obtained from data presented in Fig. 9 (—) using a FFT-IFFT sequence and the best-fit simulated components (--). Parameters: $D_0 = D_R = 1.04 \times 10^{-5}$ cm s^{-1}, $\alpha = 0.5$, $k = 0.01$ cm s^{-1}, $R_{meas} = 2100\ \Omega$.

protection from the atmosphere, to a previously dried and N_2 filled (vacuum line) quartz EPR tube. In a second, a ten-fold excess of $Dipp_3P$ was added to the electrolyzed solution to create an approximately 1 : 10 concentration ratio of $[Dipp_3P]^{+\bullet}$ and $Dipp_3P$. The spectra were recorded as solutions at 22 °C and in a frozen glass at −143 °C (Fig. 13). The isotropic liquid spectra show the presence of the expected doublet with a hyperfine coupling to ^{31}P of 23.9 mT (Table 6). The peak-to-peak linewidths of the spectral lines was found between 0.5 and 0.6 mT. Since ^{1}H is the only other magnetically active nucleus of significant abundance in the structure, it is likely that the wide lines are at least in part due to

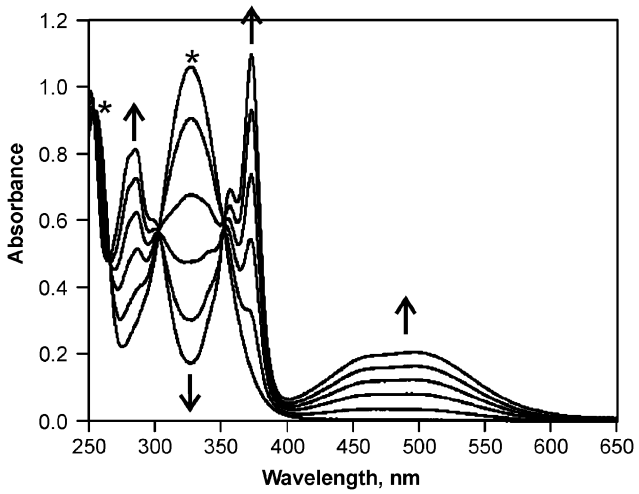

Fig. 11 Oxidation of 1.01 mM $Dipp_3P$ in CH_2Cl_2 (0.1 M $^{n}Bu_4NPF_6$) under OTTLE conditions. The initial spectrum (*) with a maximum at 375 nm is from pure $Dipp_3P$ (see Fig. 3 and Table S2, ESI†). Decrease (↓) of this band and growth (↑) of many new bands are indicated by arrows. The final spectrum with maxima at 251, 285, 357, 373, 456 and 498 nm (among others) is the spectrum of essentially pure $[Dipp_3P]^{+\bullet}$. Reduction of $[Dipp_3P]^{+\bullet}$ back to $[Dipp_3P]$ in the OTTLE cell reverses the sequence of spectra while retaining the isosbestic points.

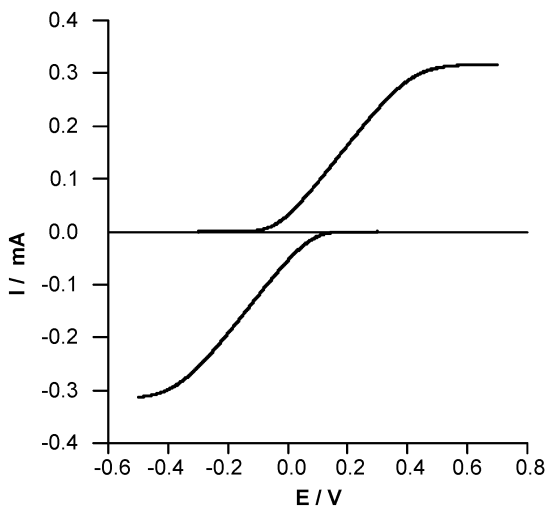

Fig. 12 RDE curves at a GC electrode before (upper) and after (lower) bulk electrolysis when $Dipp_3P^{+}$ is generated from 8.6 mM $Dipp_3P$ in CH_2Cl_2 (0.5 M $^{n}Bu_4NPF_6$). For simulations of RDE voltammograms see Fig. S6, ESI.†

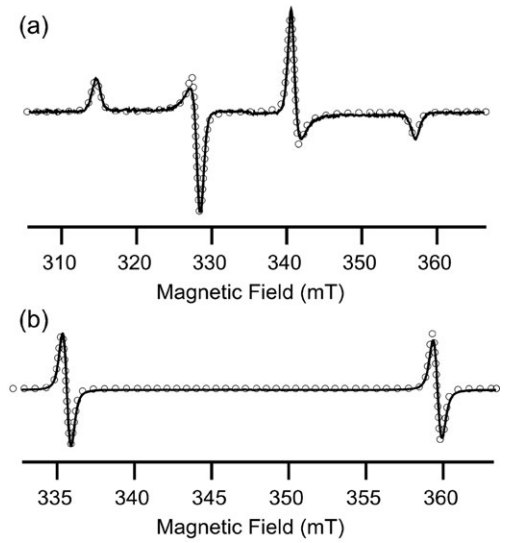

Fig. 13 Comparison of simulated (○) and experimental (—) EPR spectra obtained (a) in the glass state by freezing an electrochemically generated 1 mM solution of $Dipp_3P^+$ in CH_2Cl_2 (0.1 M $^nBu_4NPF_6$) at 130 K, and (b) at 295 K in CH_2Cl_2 using a solution prepared by $AgClO_4$ oxidation of $Dipp_3P$. Simulations performed with WinEPR software; for (a) 40% Lorentzian–60% Gaussian lineshape, $LW\perp$ = 1.0, $LW\parallel$ = 1.1 mT; for (b) with Lorentzian lines, LW = 0.12 mT and additional hfc to 6 ^1H = 0.17 mT and 6 ^1H = 0.10 mT.

unresolved proton hyperfine coupling.[36a,51] Using the program WinSim,[52] it was possible to get a superb fit using purely Lorentzian lines (as expected if all coupling is accounted for) by including two sets of six equivalent ^1H hfc of 0.17 mT (possibly isopropyl methine H) and 0.10 mT (possibly the *meta* aromatic H) and a residual LW of only 0.12 mT.[53] No measurable difference in the line width was observed between the two samples that contained on the one hand 100% $[Dipp_3P]^{+\bullet}$ and the 1:10 mixture of $[Dipp_3P]^{+\bullet}/Dipp_3P$, indicating that line broadening through intermolecular electron transfer is not significant for this system. In the frozen glass, a characteristic axially-symmetric powder pattern was obtained with parallel and perpendicular hfc tensor components of 12.7 and 42.6 mT, and a small asymmetry in the *g* tensor.[12,36,54]

The successful electrochemical generation of solutions containing $Dipp_3P^{+\bullet}$ and the demonstration of their stability on the time scale of bulk electrolysis (*i.e.* hours in CH_2Cl_2 solution at room temperature) suggested that chemical oxidation of $Dipp_3P$ should be possible. The reversible potential of the $[Dipp_3P]^{+/0}$ couple is at +0.09 V *vs.* $Fc^{+/0}$, and no further oxidation occurs until +1.25 V *vs.* $Fc^{+/0}$. The list of potential chemical oxidizing agents provided by Connelly and Geiger[55] advises that Ag(I) ion in CH_2Cl_2 solution should be a suitable oxidant at the $Ag^{+/0}$ redox couple of +0.65 V *vs.* $Fc^{+/0}$.[56] This is an attractive reagent because the by-product is expected to precipitate as solid silver. We have therefore used $AgClO_4$, $AgPF_6$ and $AgSbF_6$ as chemical oxidants to generate solutions of $[Dipp_3P^{+\bullet}]X^-$ (X^- = ClO_4^-, PF_6^-, SbF_6^-) salts in CH_2Cl_2. EPR spectra of dilute solutions of such chemically generated radicals are identical to those prepared by electrochemical methods.

Discussion

$Dipp_3P$

Structure. Since the first X-ray diffraction structure determination of Mes_3P by Mislow and co-workers,[57] it has been recognized that bulky substituents cause substantial distortions in the structure of the putative pyramidal R_3P group. Thus while PH_3 (cone angle 87°) has internal angles of 93.6°,[58] Mes_3P has greatly enlarged internal angles (average 109.7°).[36b,57] The small bond angles of PH_3 have long intrigued chemists and theoreticians. Molecular orbital theory has been used to advance a convincing explanation in the form of Walsh diagrams (Fig. S8, ESI†) that correlate the planar D_{3h} geometry for EH_3 molecules with the strongly pyramidalized C_{3v} geometry such as PH_3 adopts.[51b,59] Pyramidalization occurs when the $2a_1$ orbital (labeled as in the lower-symmetry point group; an empty p_z atomic orbital of E, for example, in planar AlH_3, and the "lone pair" orbital of EH_3, for example in PH_3) is occupied, because rehybridization of this orbital allows for partial bonding to the σ orbitals of the three substituents at E. The stabilization of $2a_1$ often provides the main energetic driving force favoring the pyramidal geometry, while 1e is destabilized to a lesser extent. In this analysis, the much greater pyramidalization of PH_3 compared to NH_3 can be traced to the lower electronegativity of the third row element, and hence reflects the fundamental identities of the central elements N and P. When substituents of high steric

Table 6 EPR parameters for $Ar_3P^{+\bullet}$ radicals

Compound	Conditions	g_{iso}	a_{iso}/mT	$g_\parallel$	$a_\parallel$/mT	$g_\perp$	$a_\perp$/mT
$Dipp_3P^{+\bullet}$	CH_3CN/295 K (*in situ*)[a]	2.008	23.9				
	CH_2Cl_2/295 K[b]	2.008	23.9				
	CH_2Cl_2/77 K[c]	*2.007*	*22.7*	2.0045	42.6	2.0085	12.7
	CH_2Cl_2/295 K[d]	2.008	23.9				
$Tripp_3P^{+\bullet}$	CH_2Cl_2/293 K[e]	2.007	23.7	2.002	41.7	2.009	13.0
$Duryl_3P^{+\bullet}$	C_3H_7CN/77 K[f]	2.0052	23.7		42.0		15.0
$Xyl_3P^{+\bullet}$	CH_3CN/123 K[f]	2.0052	24.4		41.1		17.0
$Mes_3P^{+\bullet}$	C_3H_7CN/77 K[g]	2.0052	24.0		40.2		17.1
$Ph_3P^{+\bullet}$	$CFCl_3$/77 K[f]	2.006	29.9		45.2		22.3

[a] Saturated solution (between 1×10^{-4} and 1×10^{-3} M) in CH_3CN containing 0.1 M $^nBu_4NPF_6$ at 295 K. LW_{Lo} 0.57; LW_{Hi} 0.60 mT. [b] 7.7×10^{-4} M in CH_2Cl_2 containing 0.1 M $^nBu_4NPF_6$ at room temperature. LW_{Lo} 0.54; LW_{Hi} 0.59 mT. [c] Sample as in *b* but cooled to 130 K; $g = (g_\parallel + 2g_\perp)/3$; $a = (a_\parallel + 2a_\perp)/3$.[54c] [d] Prepared from a dilute solution of $Dipp_3P$ in CH_2Cl_2 by chemical oxidation with solid $AgClO_4$. LW_{Lo} 0.57; LW_{Hi} 0.60 mT. [e] Chemical oxidation with $AgClO_4$.[12] [f] Prepared by electrolysis.[54d] [g] Electrolysis in *n*-butyronitrile.[36a]

pressure are placed on R_3P, orbital hybridization will resist the tendency towards flattening. These opposing tendencies cause *inter alia* the strong displacement of the P atom out of the plane of the aryl rings, as well as a similar distortion of the *ipso* C. Thus there seems to be a limit to the amount of planarization that can be imposed at P by bulky (carbon-based) substituents.[60]

Solid-state NMR. When Mes_3P is crystallized from ethanol/toluene, a polymorph in the space group *Cc* is obtained in which the phosphorus atom positions are disordered by an undetermined mechanism.[36b] Recrystallization from $CHCl_3$ produces a different polymorph (space group $P\bar{1}$) which has two independent molecules in the unit cell. Penner and Wasylishen detected the polymorphism of Mes_3P through the discovery of three ^{31}P resonances in the CP-MAS spectra of commercial Mes_3P.[61] Recrystallization from chloroform removed the broadest ($\Delta\nu_{1/2}$ = 49 Hz) of these lines and left behind two very sharp ($\Delta\nu_{1/2}$ = 16 Hz) resonances in a 1 : 1 ratio which are ascribed to the two independent molecules in the asymmetric unit of the $P\bar{1}$ polymorph, in which disorder was not encountered. These workers showed that asymmetry in the shielding tensors of triaryl phosphines is caused primarily by the conformations of the aryl rings in the solid state. Where these are twisted in different orientations, or where they have substituents in *exo* as well as *endo* orientations, the ^{31}P shielding tensors are significantly asymmetric. Those phosphines that crystallize with the rings in similar (or crystallographically identical) conformations and those that have all *exo* orientations of *ortho* alkyl groups tend to have the most symmetric shielding tensors. The conformation of the three Dipp rings is identical in $Dipp_3P$ by crystallographic symmetry in space group *R*3, so that the shielding tensor in absence of other phenomena ought accordingly to be cylindrically symmetric. That the spectra obtained have lines wider ($\Delta\nu_{1/2}$ = 170 Hz) than those of the monoclinic (disordered), and much wider than the triclinic phase of Mes_3P, is thus likely a reflection of the twinning by merohedry (see Structure from X-ray crystallography, above).

Photophysics. Triphenylphosphine is remarkable for the unexpectedly large Stokes shift that is observed in its fluorescence spectrum (Table S2, ESI†).[35] Changenet *et al.* have argued that this Stokes shift of ~225 kJ mol^{-1} in ethanol reflects its high barrier to pyramidal inversion because the $Ph_3P^{\ddagger}$ excited state geometry is expected to be planar or close to planar.[35a] Thus, in $Ph_3P{=}O$ which cannot go planar, the Stokes shift in ethanol is only 29 kJ mol^{-1} and on the reasonable assumption that Ph_3P has a quite similar electronic structure to that of its oxide, an upper limit for its pyramidalization energy was found to be <200 kJ mol^{-1}.[36b] These estimates can be compared to a barrier for pyramidal inversion of 147 kJ mol^{-1} obtained from HF/6-31G(d)/6-31G *ab initio* molecular orbital calculations.[62] In the case of $Dipp_3P$, there is no corresponding oxide available to index the Stokes shift as done for Ph_3P; thus we can only conclude that the barrier to pyramidal inversion is expected to be <100 kJ mol^{-1} in hexane solution. Using DFT methods, we have calculated a barrier to a planar "transition state" of only 37.5 kJ mol^{-1} in the gas phase. For more detailed insight into this phenomenon in condensed phases, we turn now to the solution dynamics as measured by NMR.

Solution dynamics. Slow dynamics processes in crowded triarylphosphines have been investigated previously by NMR methods.[5b,63–65] Rieker and Kessler,[63] supported later by Mislow and co-workers,[57] argued that the correct mechanism for exchange in Mes_3P is by a "two-ring flip" mechanism, a kind of turnstile-motion in which the rotation of one of the three aryl rings induces a flip of the remaining two to achieve the opposite propeller rotation. Stepanov *et al.* obtained a lower activation energy in $Duryl_3P$, and used this as an argument that the latter phosphine undergoes pyramidal inversion instead of ring-flipping.[64] Bellamy *et al.* have confirmed the value of about 44.5–45.6 kJ mol^{-1} for the propeller reversal in Mes_3P.[65] Based on Kessler's concept of measuring the steric interactions between the *ortho* groups in congested propeller molecules of this type, it would be expected that the considerably larger ^{i}Pr groups in $Dipp_3P$ and $Tripp_3P$ should lead to a significantly higher barrier for P–C_{ipso} bond rotation, whereas we have measured barriers by DNMR of only 49 ± 1 kJ mol^{-1}.

In an elegant study on the quaternary cation $[Mes_3PCH_3]^+$ in presence of a chiral resolving agent, Laleu *et al.* have recently provided direct experimental evidence for the two ring-flip mechanism.[9] However, this approach is not possible for neutral $Dipp_3P$, as such chiral recognition depends on ionic charges. We have instead undertaken a detailed *ab initio* computational study in which one of the Dipp groups was forced to rotate about the P–C1 bond with respect to dihedral angle θ (C1′–P–C1–C2) as defined in Scheme 1, while one other dihedral angle ϕ (C1–P–C1″–C2″) was held constant, and the remainder of the molecule was allowed to relax. From a full investigation of the energy surface resulting from varying θ in steps for different ϕ, the *only* low-energy path that interconverts species appears to be pyramidal inversion (Fig. 14).

The dark blue zones in Fig. 14 correspond to two equal energy C_3 conformations ($\theta = \phi = -83°$ and $-19°$) which are related to each other by pyramidal inversion *without* racemization (an equivalent energy surface exists for the enantiomeric structure which we have not calculated in detail.) The red zones represent a very high energy wall surrounding the whole enantiomeric surface. The process starts out as a turnstile mechanism, where the neighboring rings are made to rotate in opposite directions, but at a particular point along

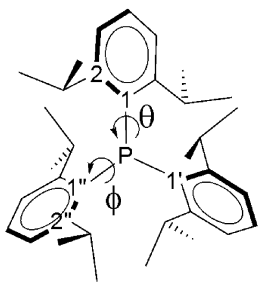

Scheme 1

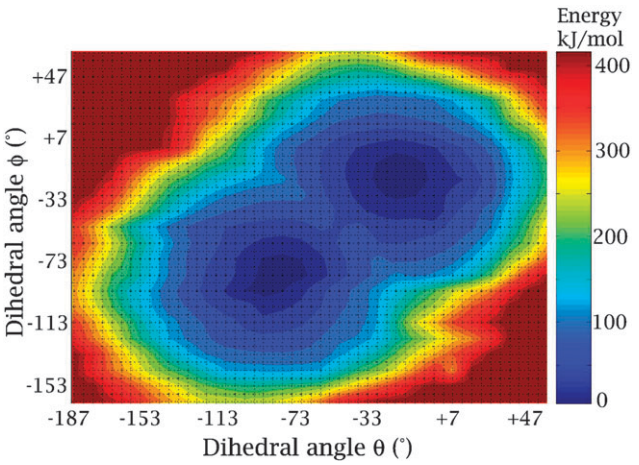

Fig. 14 Interpolated surface of the potential energy of $Dipp_3P$ as a function of the dihedral angles θ and ϕ (see text for definitions).

the way, a severe steric clash between the isopropyl groups of neighboring Dipp rings prevents further rotation. This clash apparently has a much larger energy demand than phosphorous inversion, which subsequently follows instead of completing the full rotation. The trajectory followed by the molecule along the lowest-energy pathway (Fig. 15) between the two minima passes through a saddle-point corresponding to a planar transition state ($\theta = \phi = -56°$); hence, rotation *induces* inversion[66] in very bulky triaryl phosphines. The calculated barriers to inversion of 54 kJ mol^{-1} at the HF/3-21G and 37.5 kJ mol^{-1} at B3LYP/6-31G(d) levels of theory are in reasonable agreement with the 51–53 kJ mol^{-1} obtained from the DNMR experiments. Thus when steric pressure is severe, the normal resistance to inversion at phosphorus can apparently be overcome even with carbon-based substituents.[60]

Electrochemistry. The exhaustive studies presented above confirm that $Dipp_3P$ in both CH_3CN and CH_2Cl_2 displays a chemically reversible one-electron oxidation which is, however, marked by somewhat slow electron transfer kinetics.

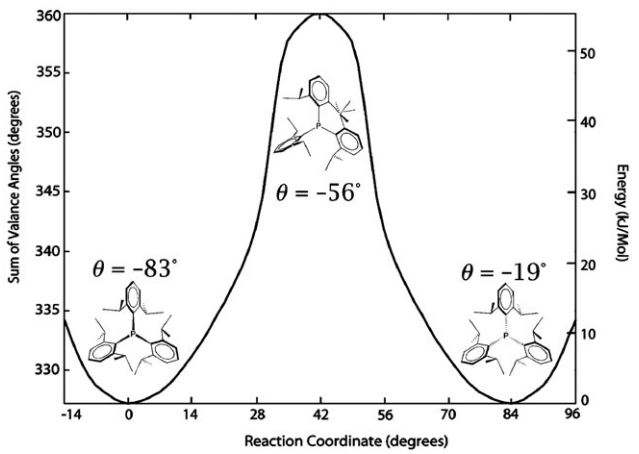

Fig. 15 A reaction coordinate (in arbitrary units) showing the lowest-energy path connecting the degenerate ground state *via* the planar transition state. The dihedral angles θ corresponding to minima and maximum are indicated.

Tordo and co-workers have determined fast electron transfer kinetics ($k_S > 1$ cm s^{-1}) for the $Mes_3P^{0/+}$ couple.[44] If this is correct, re-organizational geometry changes upon oxidation cannot be a cause of the slower electron transfer in $Dipp_3P$, as even greater changes are predicted for $Mes_3P^{+\bullet}$. A possible origin for slower electron transfer in the $Dipp_3P^{+/0}$ redox couple is, we suggest, the encapsulating nature of the isopropyl groups surrounding phosphorus, leaving a narrow channel that affords the only access to the central P atom. Moreover, at RT in solution, the DNMR results just discussed suggest rapid pyramidal inversion, which has the effect of blocking even further the access (or egress) of the electron from the P atom. An idea of this can be obtained from a diagram taken of the DFT computed planar inversion state, which is shown in Fig. 16. In EPR studies of 10% $Dipp_3P^{+\bullet}$ in presence of unoxidized $Dipp_3P$ we found no evidence of line broadening ascribed to intermolecular electron transfer. This lends additional support to the notion of rather slow electron transfer.

Comparison of phosphine redox potentials. There is a considerable body of literature on the redox chemistry or triarylphosphines.[7h,12,49,54,67] Triphenylphosphine is irreversibly oxidized at a potential of +1.04 V (anodic peak potential *vs.* $Fc^{+/0}$) in CH_3CN (our data). A small selection of the many previously reported potential values is presented in Table 7. It becomes immediately obvious that serious problems associated with use of different reference potential scales affect the published data. We have therefore re-measured the compounds listed in Table 7 in both CH_3CN and CH_2Cl_2 solutions using a common internal standard: the $Cc^{+/0}$ couple;[46] and quote our data on the Fc scale as recommended by IUPAC.[68]

In our hands, the $Dipp_3P^{+/0}$ couple in CH_2Cl_2 solution is found to be 0.15 V less cathodic than the isosteric $Tripp_3P^{+/0}$. This difference is likely due to the inductive influence of the three ^{i}Pr groups in the *para* position in $Tripp_3P$ that are missing in $Dipp_3P$, or approximately 0.05 V per ^{i}Pr group. Similarly the potentials of $Xyl_3P^{+/0}$ and $Mes_3P^{+/0}$ differ by 0.15 V, thus ~0.05 V per methyl group. Such "voltammetric

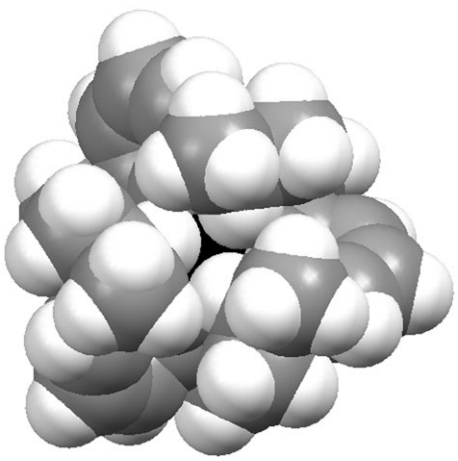

Fig. 16 View perpendicular to the three-fold rotation axis of the B3LYP/6-31G(d) calculated structure of the "transition state" geometry held to D_3 point symmetry. The van der Waals radii scale is the same as that used in the preliminary communication.[14] The phosphorus surface is rendered in black.

Table 7 Comparative redox potentials for triaryl phosphines[a]

Compound	CH_2Cl_2[b]	CH_3CN[c]	Tordo[d]	Sasaki[e]	$\sum\{\angle CPC\}$[f]	E(HOMO)[f]/eV
Ph_3P	(+0.88)	(+1.04)	(+1.400)	+1.03	310.00	−8.00
$Anthr_3P$	+0.30	(+0.37)	—	—	334.10	−6.67
Xyl_3P	+0.34	+0.40	+0.885	—	330.51	−7.31
Mes_3P	+0.19	+0.26	+0.784	+0.41	330.33	−7.20
$Dipp_3P$	+0.09	+0.18	—	—	337.01	−7.29
$Tripp_3P$	−0.06	+0.04	—	+0.16	336.80	−7.13

[a] Calculated by cyclic voltammetry from the average of oxidation and reduction peak potentials, scan rate = 0.2 V s^{-1}; values in parenthesis are E^{ox} peak potentials. [b] In CH_2Cl_2 at Pt a electrode containing 0.4 M in $^nBu_4NPF_6$ and 1 mM in analyte, *vs.* $Fc^{+/0}$, measured against $Cc^{+/0}$, expressed *vs.* $Fc^{+/0}$ by subtracting 1.35 V.[46] [c] In CH_3CN at a Pt electrode containing 0.1 M in $^nBu_4NPF_6$ and 1 mM in analyte, measured against $Cc^{+/0}$, expressed *vs.* $Fc^{+/0}$ by subtracting 1.35 V.[46] [d] In $CH_3CH_2CH_2CN$ 0.1 M in $^nBu_4NPF_6$ and 1 mM in analyte, *vs.* SCE.[36a] [e] In CH_2Cl_2 0.1 M in $^nBu_4ClO_4$ measured against a pseudo-$Ag^{+/0}$ reference electrode.[12] [f] From HF/6-31G(d) calculations.[14]

inductive influences'' are well known in metallocene chemistry.[69] Using a very extensive range of electrochemical measurements, Tordo and co-workers demonstrated a distinct influence on triarylphosphine oxidation potentials by the degree of pyramidalization[70] at phosphorus through a careful consideration of isosteric species and by eliminating the inductive effects of substituents.[36a,51b] At the same time, these workers have pointed out the significance of substituent inductive effects and showed that good correlations with Hammett parameters could be obtained when the phosphines with, and those without, *para* substituents are treated separately.[51b] Since the inductive effects on redox potentials of ^{i}Pr and Me groups in this system are the same, the significant Mes/Tripp (−0.25 V) and Xyl/Dipp (−0.25 V) shifts do seem to be mainly due to the structural changes induced by the *ortho* ^{i}Pr groups, but whether this is truly from planarization or from activation by distortion is difficult to decide (see under Structure of $Dipp_3P$ above).[71]

[$Dipp_3P^{+\bullet}$] radical cation

Stability. Extensive studies have shown that the end product of electrochemical oxidation of Ph_3P is always $Ph_3P{=}O$.[72] More important to this study is the fact that a detailed investigation has shown that a similar process operates for Mes_3P, where in wet or oxygenated solvents, $Mes_3P{=}O$ is formed, likely along with Mes_3PH^+.[44,73] By contrast, solutions of $Dipp_3P$ prepared in CH_3CN without special drying procedures and without purging by N_2 or Ar, display essentially identical voltammetric behavior in the 0/+1 process on the timescale of CV or RDE to that observed for carefully dried and deoxygenated solutions, although preparations of $Dipp_3P^{+\bullet}$ exposed to the atmosphere do degrade on the timescale of hours to as yet unknown products. We attribute this enhanced stability of the radical cation to the superior steric shielding afforded by the large enveloping *exo* ^{i}Pr groups. Support for this assertion is provided by the electrochemically and chemically irreversible oxidation of $Anthr_3P$ (Table 7), at considerably higher potentials, despite the approximately equal steric *pressure* of the Anthr groups compared to Dipp (consideration of $\sum\angle$(CPC) from both crystallography and computation).[14] The Anthr substituent does not provide adequate steric shielding for the phosphorus lone pair, and its electrochemical behavior is much closer to that of Ph_3P than any of Xyl_3P, Mes_3P, $Dipp_3P$ or $Tripp_3P$. Indeed, $Anthr_3P{=}O$ is a known compound,[74] whereas neither $Dipp_3P$ nor $Tripp_3P$ react with oxygen in the form of O_2 or H_2O_2.

Spectroscopy. The EPR parameters for $Dipp_3P^{+\bullet}$ (Table 6) may be compared to those of previously prepared stable and unstable $R_3P^{+\bullet}$. All the parameters are similar to, but not identical with, those of the isosteric $Tripp_3P^{+\bullet}$, suggesting that inductive effects from the alkyl groups affect the electronic properties of the radicals as well.[14] Our value for, in particular, the $a_\perp$ component of the hfc tensor is the smallest of the series presented in Table 6, and may be compared to the values recorded for $Ph_3P^{+\bullet}$, $Mes_3P^{+\bullet}$, $Xyl_3P^{+\bullet}$, $Duryl_3P^{+\bullet}$ and $Tripp_3P^{+\bullet}$.[67] Tordo has argued that this parameter indicates the degree of planarization of the phosphorus pyramid in the radical cation.[67d,e] Our gas-phase calculation on $Dipp_3P^{+\bullet}$ gives a $\angle$(CPC) value of 118.9° (Table 1), which corresponds to Tordo's "α" = 6.0°.[70] Thus the evidence from EPR spectroscopy and calculations is that excessively bulky substituents such as Dipp and Tripp cause significant flattening in $Ar_3P^{+\bullet}$.

Conclusions

Triarylphosphines with two *ortho* ^{i}Pr substituents per aryl ring are currently the most sterically congested phosphines known. They have unusual properties which include high thermal stability and volatility, stereochemical non-rigidity apparently due to the rare phenomenon of pyramidal inversion at phosphorus, and facile electrochemical oxidation. Their radical cations are extremely stable—samples of $Dipp_3P^{+\bullet}$ prepared in sealed vessels under rigorously dry conditions retain their EPR intensity for months—which is attributable primarily to the encapsulating effect of the bulky *ortho* isopropyl groups. Work in our laboratories is ongoing to delineate the reactivity of $Dipp_3P$ and to isolate stable salts of its radical cation. Thus far, all salts of $Dipp_3P^+$ that we have been able to prepare appear to be amorphous to X-rays.

Experimental

General methods

DippBr was prepared as previously reported.[75] PCl_3, anhydrous CuCl, Mg turnings and silver salts (Aldrich) were used as received. THF was distilled from sodium benzophenone immediately before use. *n*-Heptane and xylenes were distilled

from $LiAlH_4$ and Na, respectively, under N_2. Hexanes, chloroform and all deuterated solvents were used as received. All reactions were performed in an atmosphere of dry N_2 in oven-dried glassware (>4 h at >160 °C) unless otherwise noted.

$Dipp_3P$

Synthesis. To a mixture of magnesium turnings (0.56 g, 22.5 mmol), I_2 (50 mg, 0.2 mmol) and tetrahydrofuran (50 mL) was added DippBr (5.41 g, 22.5 mmol), and the mixture was stirred over night at room temperature. The resultant solution of DippMgBr[75] was cooled to −70 °C and CuCl (98%, 2.27 g, 22.5 mmol) was added under N_2. The mixture was stirred for about 1 h at −70 °C, then warmed to RT and stirred overnight, evaporated, re-dissolved in 50 mL freshly distilled *n*-heptane, the suspension cooled to −70 °C and PCl_3 (98%, 1.05 g, 0.67 mL, 7.64 mmol) added. The mixture was stirred for about 45 min at −70 °C, warmed to RT and heated to reflux for 40 h then cooled to RT. Hexanes (30 mL) was added to the mixture and the resultant suspension was filtered through Celite with suction. Evaporation of solvent left a sticky solid, which could be recrystallized from hot hexanes–chloroform to afford crystalline $Dipp_3P$ (2.33 g, 4.52 mmol, ~60% yield).[76] Calc. for $C_{36}H_{51}P$: C, 84.00; H, 9.99%. Found: C, 84.26; H, 9.71%. Mass spectrometry (EI): 514.3744 ($C_{36}H_{51}P^+$, −1.1 ppm, 100%); 471.31757 ($C_{33}H_{44}P^+$, +1.0 ppm, 9%). mp: sublimes <360 °C/1 bar. NMR data: ^1H, ^{13}C see Table 2; ^{31}P δ −49.7 w.r.t. ext. H_3PO_4.

Crystallography. Colorless blocks of $C_{36}H_{51}P$ were coated with Paratone 8277 oil (Exxon) and mounted on glass fibers. All measurements were made on a Bruker Smart CCD diffractometer with graphite monochromated Mo-Kα radiation. The data were corrected for Lorentz and polarization effects and for absorption using SADABS V2.01.[77] Crystal, solution and refinement details are reported in Table 8. Selected interatomic distances and angles are presented in Table 1 and full geometrical parameters are available in Table S1, ESI.† The solution of the structure of $Dipp_3P$ was vexed by persistent twinning by merohedry. Several diffraction data sets obtained at room temperature failed to yield satisfactory refinement. Finally, an LT dataset (193(2) K) on a very high quality crystal was obtained using ω and φ scans to a maximum θ value of 26.4°. The program ROTAX[78] was used to determine a twin law consisting of 180° rotation about the [1 1 0] direct axis direction, which allowed for solution and refinement of the structure, with twin occupancy ratio of 0.83/0.17. The non-hydrogen atoms were refined anisotropically. Hydrogen atoms were included at geometrically idealized positions and were not refined. The final cycles of full-matrix least-squares refinement using SHELXTL[79] converged. The weighting scheme was based on counting statistics and the final difference maps are essentially featureless.

CCDC reference number 660828.

For crystallographic data in CIF or other electronic format see DOI: 10.1039/b709602j

Table 8 Crystal data and structure refinement of $Dipp_3P$

Space group	*R*3
a/Å	16.5047(7)
c/Å	10.2363(9)
γ/°	120
Z	3
θ Range for data collection/°	2.45–26.40
Index ranges, *hkl*	−20 to 20, −20 to 20, −12 to 12
Total/independent reflections	5662/2205 (R_{int} = 0.0220)
Data/restraints/parameters	2205/1/113
Goodness-of-fit on F^2	1.153
Final *R* indices [$I > 2\sigma(I)$]	*R*1 = 0.0294, *wR*2 = 0.0884
R indices (all data)	*R*1 = 0.0294, *wR*2 = 0.0884

Luminescence spectroscopy. The spectrum of $Dipp_3P$ was obtained in fluorescence mode using 5.8×10^{-4} M solutions in cyclohexane and saturated solutions in 95% EtOH. A Perkin Elmer LS50B luminescence spectrometer was employed for the measurements, which are displayed on an arbitrary intensity scale in Fig. 3 (numerical data in Table S2, ESI†).

NMR spectroscopy. NMR spectra were obtained on Bruker/Tecmag AC250 (^1H, ^{13}C and ^{31}P) and Varian Innova 500 spectrometers (VT ^1H and ^{13}C). ^1H and ^{13}C spectra are referenced to (residual) solvent peaks, while ^{31}P NMR spectra were referenced to external 85% H_3PO_4 and collected either in locked mode for the purified final product or in unlocked mode when aliquots of the reactions were investigated to monitor the completeness of the reactions.

For the dynamic NMR studies, solutions of $Dipp_3P$ were prepared in CD_2Cl_2 at 10% w/v which were transferred to a 5 mm thin walled NMR tube. The low temperatures were attained using liquid N_2 as the coolant, and the output temperatures for the thermocouple were calibrated against the chemical shift difference of methanol over the appropriate temperature range.[80] Both ^1H and $\{^1H\}$–^{13}C spectra were obtained over a temperature range of 30 °C to −100 °C in 5 °C increments. Decoupled carbon spectra were recorded on samples spun at 20 Hz using a 32 kHz sweep width and a 3 μs pulse width corresponding to a tip angle of 45°. A total of 256 transients were recorded with a 1.3 s acquisition time and a 1 s recycle delay. The FID's were stored as 128 k files, and processed using standard FFT and apodizing methods using a line broadening of 0.5 Hz throughout. Proton spectra were recorded on samples spun at 20 Hz using a spectral width of 15 kHz and a pulse width of 5.95 μs corresponding to a 45° tip angle. Eight scans were recorded using a 1 s acquisition time and a 5 s recycle delay. The FID's were stored as 32 K files and processed using standard FFT and apodization methods where a line broadening of 0.1 Hz was used throughout.

The half height line widths of the appropriate lines were measured at each temperature above coalescence. Selective inversion [spectral width (5991.6 Hz), acquisition time (1.9 s), number of points (22 K), recycle delay (10.0 s) mixing time (37 step array ranging from 2 μs to 7 s), spin rate (0 Hz), no. scans (16) with gradient stabilization] and *T*1 [first delay (20 s), pulse sequence: {180°, delay times (array from 0.0625 to 32 s), 90°, acqu. (1.9 s)}, spin rate (20 Hz) and no. scans (16)] experiments for ^1H were performed at −75, −70, −65 and −60 °C. The rates of exchange were extracted using the CIFFIT program.[81] The resulting spectra were exported into MestReC[82] and were subsequently converted to ASCII format at a digital resolution of 0.1 Hz point^{-1}. The region of interest was selected from each spectrum and modeled using an in house program written

in Matlab[83] that simulates the spectral parameters of the half height line width and exchange rate which is statistically compared by superimposing the experimental spectrum on the simulated one to give the best fit.

Computation. The structure of $Dipp_3P$ was modeled using the internal geometry tools in HyperChem 7.52,[84] and optimized initially using the MM+ force field. Thereafter the semi-empirical PM3 method was used to obtain a preliminary structure. These geometries were exported to Gaussian 98 for Windows,[85] and were then refined at the HF/6-31G(d) level of theory without symmetry constraint. From this starting point, the structure of $Dipp_3P^+$ was calculated using UHF/6-31G(d) theory. The geometry of $Dipp_3P$ was also optimized under C_3 and D_3 point-group symmetry restraints using the B3LYP/6-31G(d) method. Geometric results are reported in Tables 1 and S1, ESI.†A detailed energy surface for the rotation-inversion process in $Dipp_3P$ was undertaken free of any symmetry restrictions. The size of the problem and the available computer resources restricted us to the HF/3-21G basis set for this extensive set of computations. The reasonableness of the model was checked by comparison of the geometries of the structures obtained in the ground state and in the transition state against the results of the higher-level calculations. Two dihedral angles involving C_{ipso}–P–C_{ipso}–C_{ortho} atoms were defined (Scheme 1). One of these angles was driven at 10° increments, while the second was fixed at 10° increments and the remainder of the molecule was allowed to relax completely. An energy surface was constructed in these two angular units, following a methodology previously reported.[66]

Electrochemistry. All voltammograms were obtained at 22 ± 2 °C in freshly distilled CH_3CN and CH_2Cl_2 solvents containing 0.1 M (unless otherwise indicated) $^nBu_4NPF_6$ as the supporting electrolyte and purged with dry N_2 for 10 min directly before use. In all experiments, except the EPR spectroelectrochemistry (see below), Pt auxiliary and silver/silver chloride reference electrodes, the latter separated from the bulk solution by a fine-porosity frit, were employed in a three-electrode arrangement; dc measurements were undertaken with either BioAnalytical Systems CV-50 or 100B computer-controlled potentiostats, and simulations of the voltammograms were performed using DigiSim software.[86] Pt, Au and GC macrodisk electrodes and Pt and GC microelectrodes of known area and radii were used as working electrodes in stationary electrode experiments. The working electrodes were polished with 0.3 μm alumina on a clean polishing cloth (Buehler, USA), rinsed with water, and dried with tissue paper. For rotating disk electrode (RDE) voltammetry, 3 mm diameter GC macrodisk electrodes were used with a Metrohm Model 628–10 RDE accessory in conjunction with a BAS potentiostat. Bulk electrolysis was performed with the BAS 100B potentiostat using two concentric Pt gauze basket electrodes in a cell described elsewhere.[47] Reference potential calibration was performed against the $Cp^*_2Fe^{+/0}$ (Cp^*_2Fe = decamethylferrocene) and $Cc^{+/0}$ (Cc = cobaltocene) redox couples, and potentials are quoted on the $Fc^{+/0}$ (Fc = ferrocene) scale. Details of the large amplitude Fourier Transform (FT) ac voltammetric instrumentation are described elsewhere.[17] For all these FT experiments a large amplitude (80 mV) sinusoidal waveform was superimposed onto a triangular dc potential waveform which was swept at a rate of 49.68 mV s^{-1}. Several frequencies were employed as specified, and the number of data points collected was 64 k. The experimental data, obtained with the FT form of instrumentation, yield current, time and applied potential as the output information. The FT algorithm converts the time domain to the frequency domain to give power spectra. The inverse FT operation then separates the data into dc and harmonic components.

Spectroelectrochemistry. *In situ* electronic spectroelectrochemical experiments were conducted in a 10 × 1 mm i.d. quartz cell. A coarse Pt mesh working electrode was used for electrolysis and a Cary 5 UV-Vis-NIR spectrophotometer was used to obtain electronic spectra under an atmosphere of N_2 gas at 20 ± 2 °C. *In situ* EPR electrochemistry experiments were conducted using Au micromesh electrodes[87] in a conventional EPR flat cell on Bruker ER200D and ESP300E instruments at X-band frequencies. An EG&G 273 potentiostat was used to generate the radical cation using an applied potential 0.1 V more positive than the peak potential *vs.* a Cu wire quasi-reference electrode.

EPR spectroscopy. Solutions of the analyte were prepared *ex situ* in a bulk electrolysis cell as described above. In one experiment, an aliquot of a solution prepared by the exhaustive electrolysis of 10.00 mL of 1.0 × 10^{-3} M solution in CH_2Cl_2 (0.1 M in $^nBu_4NPF_6$) was placed in a conventional 4 mm cylindrical quartz EPR cell. The remaining solution was made 1.0 × 10^{-2} M in $Dipp_3P$ to give ~10 : 1 ratio of neutral to oxidized material. EPR spectra were recorded at 295 and at 130 K on a Bruker E380E spectrometer operating at 9.43 GHz in CW mode. Microwave frequencies were determined with an EIP 548A frequency counter, and *g* values are measured against the F^+ line of CaO (2.0001 ± 0.0002).[88] Samples were also prepared by the addition of an excess of $AgClO_4$, $AgPF_6$ and $AgSbF_6$ to solid $Dipp_3P$ in "T" cells consisting of a 4 mm Pyrex EPR tube fused at a 75° angle to an 8 mm Pyrex reaction tube. CH_2Cl_2 was vacuum distilled onto the solid mixture, and the tube was flame sealed. Upon melting, an immediate colour change to cherry red was observed. The EPR cell was filled with solutions of the $[Dipp_3P^+]X^-$ salts in CH_2Cl_2, and the concentration was reduced by internal distillation of the solvent so that the spectra were close to the detection limit of the instrument. In this way, the effect of concentration broadening on the EPR linewidths was assumed to be eliminated. These spectra were obtained on a Bruker EMX 113/10 instrument also operating at X band at 18 ± 2 °C. Simulations of the EPR spectra were conducted using Bruker SimFonia (v. 1.25)[89] and PEST WinSim (v. 0.98) software.[52]

Acknowledgements

We thank the Natural Sciences and Engineering Research Council (Canada) and the Australian Research Council for funding. An ARC Linkage-International grant (2003–2005) facilitated this collaboration. The assistance of Si-Xuan Goh with some of the electrochemical experiments is gratefully

acknowledged. G. Wolmershauser, M. Parvez and R. Macdonald are thanked for obtaining X-ray data sets; J. Boas and R. Webster assisted with collection of EPR data. C. Campana of Bruker Analytical X-ray is thanked for help with solving the twinning problem. G. Lin and D. Iuga obtained the solid state ^{31}P NMR spectra.

References

1 IUPAC recommendation for R_3P is *phosphane*. The widespread use of *phosphine* in the English speaking world leads us to use this non-IUPAC term.

2 (*a*) C. A. Tolman, *Chem. Rev.*, 1977, **77**, 313–348; (*b*) C. A. Tolman, *J. Am. Chem. Soc.*, 1970, **92**, 2956–2965; (*c*) N. G. Andersen and B. A. Keay, *Chem. Rev.*, 2001, **101**, 997–1030; (*d*) A. L. Fernandez, M. R. Wilson, A. Prock and W. P. Giering, *Organometallics*, 2001, **20**, 3429–3435; (*e*) S. Joerg, R. S. Drago and J. Sales, *Organometallics*, 1998, **17**, 589–599; (*f*) A. Fernandez, C. Reyes, M. R. Wilson, D. C. Woska, A. Prock and M. P. Giering, *Organometallics*, 1997, **16**, 342–348.

3 (*a*) R. A. Stockland, M. C. Kohler, I. A. Guzei, M. E. Kastner, J. A. Bawiec, D. C. Labaree and R. B. Hochberg, *Organometallics*, 2006, **25**, 2475–2485; (*b*) V. A. Zagumennov and E. V. Nikitin, *Russ. J. Electrochem.*, 2003, **39**, 1236–1239; (*c*) R. C. Bott, G. A. Bowmaker, R. W. Buckley, P. C. Healy and M. C. S. Perera, *Aust. J. Chem.*, 2000, **53**, 175–181; (*d*) A. Bayler, A. Schiera and H. Schmidbaur, *Inorg. Chem.*, 1998, **37**, 4353–4359; (*e*) A. Bayler, A. Schier, G. A. Bowmaker and H. Schmidbaur, *J. Am. Chem. Soc.*, 1996, **118**, 7006–7007.

4 Abbreviations used in this paper. Dipp: 2,6-diisopropylphenyl. Duryl: 2,3,5,6-tetramethylphenyl. Mes: 2,4,6-trimethyphenyl. Mes*: 2,4,6-tri-*tert*-butylphenyl. Tripp: 2,4,6-triisopropylphenyl. Xyl: 2,6-dimethylphenyl. RT: room temperature, 22 °C unless otherwise specified. LT: low temperature. VT: variable temperature. LW: line-width. EI: electron impact. dc: direct current. ac: alternating current. GC: glassy carbon. RDE: rotating disk electrode. FT: Fourier transform. EPR: electron paramagnetic resonance. SS: solid state. MAS: magic angle spinning. CP: cross-polarization. $\Delta\nu_{1/2}$: full-width at half height. Fc: ferrocene, Cp_2Fe. Cc: cobaltocene, Cp_2Co, Cp: η^5-C_5H_5. Cp*: η^5-$C_5(CH_3)_5$. hfc: hyperfine coupling. LSA: line shape analysis. CV: cyclic voltammetry. SCE: aqueous saturated calomel electrode.

5 (*a*) E. C. Alyea, G. Ferguson, J. F. Gallagher and J. Malito, *Acta Crystallogr., Sect. C*, 1993, **49**, 1473–1476; (*b*) A. Bayler, G. A. Bowmaker and H. Schmidbaur, *Inorg. Chem.*, 1996, **35**, 5959–5960; (*c*) E. C. Alyea, G. Ferguson and S. Kannan, *Polyhedron*, 2000, **19**, 2211–2213; (*d*) R. C. Bott, G. A. Bowmaker, R. W. Buckley, P. C. Healy and M. C. S. Perera, *Aust. J. Chem.*, 2000, **53**, 175–181.

6 (*a*) S. Sasaki and M. Yoshifuji, *Curr. Org. Chem.*, 2007, **11**, 17–31; (*b*) J. C. Lee, M. G. Wang and F. E. Hong, *Eur. J. Inorg. Chem.*, 2005, 5011–5017; (*c*) J. C. Hierso, A. Fihri and R. Amardeil, *Tetrahedron*, 2005, **61**, 9759–9766; (*d*) D. Alberti, R. Goddard and K. R. Porschke, *Organometallics*, 2005, **24**, 3907–3915; (*e*) F. E. Hong, Y. J. Ho and Y. C. Chang, *J. Organomet. Chem.*, 2005, **690**, 1249–1257; (*f*) A. Yahav, I. Goldberg and A. Vigalok, *Inorg. Chem.*, 2005, **44**, 1547–1553; (*g*) S. Ogoshi, M. Ueta, M. Oka and H. Kurosawa, *Chem. Commun.*, 2004, 2732–2733; (*h*) F. Bellina, A. Carpita and R. Rossi, *Synthesis (Stuttgart)*, 2004, 2419–2440; (*i*) R. C. Smith and J. D. Protasiewicz, *Organometallics*, 2004, **23**, 4215–4222; (*j*) M. Jimenez-Tenorio, M. C. Puerta, I. Salcedo, P. Valerga, S. I. Costa, L. C. Silva and P. T. Gomes, *Organometallics*, 2004, **23**, 3139–3146; (*k*) A. S. King, G. Ferguson, J. F. Britten and J. F. Valliant, *Inorg. Chem.*, 2004, **43**, 3507–3513; (*l*) G. Canepa, C. D. Brandt and H. Werner, *Organometallics*, 2004, **23**, 1140–1152; (*m*) H. Werner, *Dalton Trans.*, 2003, 3829–3837; (*n*) T. Matsumoto, T. Kasai and K. Tatsumi, *Chem. Lett.*, 2002, 346–347.

7 (*a*) C. Dutan, S. Shah, R. C. Smith, S. Choua, T. Berclaz, M. Geoffroy and J. D. Protasiewicz, *Inorg. Chem.*, 2003, **42**, 6241–6251; (*b*) A. Matni, L. Boubekeur, N. Mezailles, P. Le Floch and M. Geoffroy, *Chem. Phys. Lett.*, 2005, **411**, 23–27; (*c*) C. Gouverd, M. Brynda, T. Berclaz and M. Geoffroy, *J. Organomet. Chem.*, 2006, **691**, 72–78; (*d*) P. Adkine, T. Cantat, E. Deschamps, L. Ricard, N. Mezailles, P. Le Floch and M. Geoffroy, *Phys. Chem. Chem. Phys.*, 2006, **8**, 862–868; (*e*) T. Sasamori, E. Mieda, N. Nagahora, K. Sato, D. Shiomi, T. Takui, Y. Hosoi, Y. Furukawa, N. Takagi, S. Nagase and N. Tokitoh, *J. Am. Chem. Soc.*, 2006, **128**, 12582–12588; (*f*) S. Sasaki, F. Murakami and M. Yoshifuji, *Organometallics*, 2006, **25**, 140–147; (*g*) S. Sasaki, F. Murakami, M. Watanabe, K. Kato, K. Sutoh and M. Yoshifuji, *J. Organomet. Chem.*, 2005, **690**, 2664–2672; (*h*) S. Marque and P. Tordo, *Top. Curr. Chem.*, 2005, **250**, 43–76; (*i*) S. Sasaki, R. Chowhury and M. Yoshifuji, *Tetrahedron Lett.*, 2004, **45**, 9193–9196; (*j*) S. Sasaki, H. Aoki, K. Sutoh, S. Hakiri, K. Tsuji and M. Yoshifuji, *Helv. Chim. Acta*, 2002, **85**, 3842–3847; (*k*) F. Murakami, S. Sasaki and M. Yoshifuji, *Angew. Chem., Int. Ed.*, 2002, **41**, 2574–2576; (*l*) F. Murakami, S. Sasaki and M. Yoshifuji, *Angew. Chem., Int. Ed.*, 1999, **38**, 340–343; (*m*) K. Tsuji, S. Sasaki and M. Yoshifuji, *Tetrahedron Lett.*, 1999, **40**, 3203–3206; (*n*) S. Sasaki, F. Murakami, M. Murakami and M. Yoshifuji, *Tetrahedron Lett.*, 1997, **38**, 7095–7098.

8 (*a*) K. Sutoh, S. Sasaki and M. Yoshifuji, *Inorg. Chem.*, 2006, **45**, 992–998; (*b*) N. Nagahora, T. Sasamori and N. Tokitoh, *Chem. Lett.*, 2006, **35**, 220–221; (*c*) C. Moser, M. Nieger and R. Pietschnig, *Organometallics*, 2006, **25**, 2667–2672; (*d*) C. Moser, A. Orthaber, M. Nieger, F. Belaj and R. Pietschnig, *Dalton Trans.*, 2006, 3879–3885; (*e*) N. Nagahora, T. Sasamori, N. Takeda and N. Tokitoh, *Chem.–Eur. J.*, 2004, **10**, 6146–6151; (*f*) R. Pietschnig and E. Niecke, *Organometallics*, 1996, **15**, 891–893; (*g*) S. Kawasaki, A. Nakamura, K. Toyota and M. Yoshifuji, *Organometallics*, 2005, **24**, 2983–2987.

9 B. Laleu, G. Bernardinelli, R. Chauvin and J. Lacour, *J. Org. Chem.*, 2006, **71**, 7412–7416, and references therein.

10 (*a*) R. T. Boeré, V. Klassen and G. Wolmershäuser, *J. Chem. Soc., Dalton Trans.*, 1998, 4147–4154; (*b*) R. T. Boeré, V. Klassen and G. Wolmershäuser, *Can. J. Chem.*, 2000, **78**, 583–589; (*c*) R. E. Boeré, R. T. Boeré, J. Masuda and G. Wolmershäuser, *Can. J. Chem.*, 2000, **78**, 1613–1619; (*d*) R. T. Boeré, M. L. Cole, P. C. Junk and J. D. Masuda, *Chem. Commun.*, 2004, 2564–2565.

11 R. T. Boeré and J. D. Masuda, *Can. J. Chem.*, 2002, **80**, 1607–1617.

12 S. Sasaki, K. Sutoh, M. Murakami and M. Yoshifuji, *J. Am. Chem. Soc.*, 2002, **124**, 14830–14831.

13 A recently reported system where Tripp groups are combined with a bulky terphenyl actually has smaller sums-of-angles around phosphorus: S. Sasaki, R. Chowdhury and M. Yoshifuji, *Tetrahedron Lett.*, 2004, **45**, 9193–9196.

14 R. T. Boeré and Y. Zhang, *J. Organomet. Chem.*, 2005, **690**, 2651–2657.

15 J. A. S. Howell, J. D. Lovatt, P. McArdle, D. Cunningham, E. Maimone, H. E. Gottlieb and Z. Goldschmidt, *Inorg. Chem. Commun.*, 1998, **1**, 118–120.

16 An analysis of six crystal structures of phosphines with three equivalent, mono *ortho* substituted, aryl rings, all with substituents in the *exo* position, suggests that sufficiently bulky groups cause a *decrease* in $\sum\{\angle CPC\}$ of up to 10°; however HF/6-31G(d) calculations show a smaller effect from this "reverse" steric pressure[14].

17 (*a*) B. D. Fleming, N. L. Barlow, J. Zhang, A. M. Bond and F. A. Armstrong, *Anal. Chem.*, 2006, **78**, 2948–2956; (*b*) D. J. Gavaghan and A. M. Bond, *Electroanalysis*, 2006, **18**, 333–344; (*c*) A. A. Sher, A. M. Bond, D. J. Gavaghan, K. Gillow, N. W. Duffy, S. X. Guo and J. Zhang, *Electroanalysis*, 2005, **17**, 1450–1462; (*d*) B. D. Fleming, J. Zhang, A. M. Bond, S. G. Bell and L. L. Wong, *Anal. Chem.*, 2005, **77**, 3502–3510; (*e*) A. M. Bond, N. W. Duffy, S. X. Guo, J. Zhang and D. Elton, *Anal. Chem.*, 2005, **77**, 186A–95A; (*f*) A. A. Sher, A. M. Bond, D. J. Gavaghan, K. Harriman, S. W. Feldberg, M. W. Duffy, S. X. Guo and J. Zhang, *Anal. Chem.*, 2004, **76**, 6214–6228; (*g*) J. Zhang, S. X. Guo, A. M. Bond and F. Marken, *Anal. Chem.*, 2004, **76**, 3619–3629.

18 P. P. Power, *Chem. Rev.*, 2003, **103**, 789–809. As defined herein, a distinction is made between free radicals that are inherently *stable* as isolated species, which do not decompose at RT under an inert atmosphere, and *persistent* radicals which have a relatively long lifetime under the conditions under which they are generated.

19 A. Armstrong, T. Chivers and R. T. Boeré, in *Modern Aspects of Main Group Chemistry*, ed. M. Lattman and R. A. Kemp, ACS Symp. Ser., American Chemical Society, Washington, DC, 2006, vol. 917, pp. 66–80.

20 (*a*) S. L. Hinchley, C. A. Morrison, D. W. H. Rankin, C. L. B. Macdonald, R. J. Wiacek, A. H. Cowley, M. F. Lappert, G. Gundersen, J. A. C. Clyburne and P. P. Power, *Chem. Commun*., 2000, 2045–2046; (*b*) S. L. Hinchley, C. A. Morrison, D. W. H. Rankin, C. L. B. Macdonald, R. J. Wiacek, A. Voigt, A. H. Cowley, M. F. Lappert, G. Gundersen, J. A. C. Clyburne and P. P. Power, *J. Am. Chem. Soc*., 2001, **123**, 9045–9053.

21 (*a*) S. Loss, A. Magistrato, L. Cataldo, S. Hoffmann, M. Geoffroy, U. Rothlisberger and H. Grutzmacher, *Angew. Chem., Int. Ed*., 2001, **40**, 723–726; (*b*) L. Cataldo, C. Dutan, S. K. Misra, S. Loss, H. Grutzmacher and M. Geoffroy, *Chem.–Eur. J*., 2005, **11**, 3463–3468.

22 Y. Canac, A. Baceiredo, W. W. Schoeller, D. Gigmes and G. Bertrand, *J. Am. Chem. Soc*., 1997, **119**, 7579–7580.

23 (*a*) A. Armstrong, T. Chivers, M. Parvez and R. T. Boeré, *Angew. Chem*., 2004, **116**, 508–511; (*b*) A. Armstrong, T. Chivers, M. Parvez and R. T. Boeré, *Angew. Chem., Int. Ed*., 2004, **43**, 502–505; (*c*) A. Armstrong, T. Chivers, M. Parvez, G. Schatte and R. T. Boeré, *Inorg. Chem*., 2004, **43**, 3453–3460; (*d*) A. Armstrong, T. Chivers, H. M. Tuononen, M. Parvez and R. T. Boeré, *Inorg. Chem*., 2005, **44**, 7981–7991.

24 W. Kaim, H. Bock and H. Nöth, *Chem. Ber*., 1978, **111**, 3276–3279.

25 (*a*) R. G. Hicks and R. Hooper, *Inorg. Chem*., 1999, **38**, 284–286; (*b*) R. G. Hicks, L. Ohrstrom and G. W. Patenaude, *Inorg. Chem*., 2001, **40**, 1865–1870; (*c*) T. Barclay, R. G. Hicks, A. S. Ichimura and G. W. Patenaude, *Can. J. Chem*., 2002, **80**, 1501–1506.

26 P. Agarwal, N. A. Piro, K. Meyer, P. Müller and C. C. Cummins, *Angew. Chem., Int. Ed*., 2007, **46**, 3111–3114.

27 O. V. Parakin, E. V. Nikitin, Yu. A. Ignat'ev, A. S. Romakhin, Yu. M. Kargin, A. V. Il'yasov, A. A. Vafina, G. V. Romanov and A. N. Pudovik, *J. Gen. Chem. USSR*, 1984, **55**, 1058.

28 R. T. Boeré, J. D. Masuda and P. Tran, *J. Organomet. Chem*., 2006, **691**, 5597–5603.

29 Direct reaction of DippMgBr with PCl_3 in THF produced a complex reaction mixture, among which $\{DippP\}_3$ and $\{DippP\}_4$ are major constituents (NMR and crystallographic evidence). The synthesis of $\{Tripp_2P\}_2$ is reported to form from reaction of PCl_3 with TrippLi in reasonable yield and in poor yield from TrippMgBr: F. J. Brady, C. J. Cardin, D. J. Cardin and D. J. Wilcock, *Inorg. Chim. Acta*, 2000, **298**, 1–8. Two Tripp groups can be introduced cleanly into R_2PCl using conventional lithium reagents,[7g] but the third substitution requires an organocopper reagent.[12] We attribute the effectiveness of ArCu reagents to the suppression of electron-transfer which induces P–P coupling reactions.

30 A. Aranyos, D. W. Old, A. Kiyomori, J. P. Wolfe, J. P. Sadighi and S. L. Buchwald, *J. Am. Chem. Soc*., 1999, **121**, 4369–4378.

31 S. J. Greenfield and S. R. Gilbertson, *Synthesis (Stuttgart)*, 2001, 2337–2340.

32 F. Langer, K. Pünterer, R. Stürmer and P. Knochel, *Tetrahedron: Asymmetry*, 1997, **8**, 715–738.

33 H.-F. Grützmacher and D. Kirchhoff, *Organometallics*, 2001, **20**, 3738–3744.

34 (*a*) M. Nespolo and G. Ferraris, *Acta Crystallogr., Sect. A*, 2004, **60**, 89–95; (*b*) M. Nespolo and G. Ferraris, *Z. Kristallogr*., 2003, **218**, 178–181.

35 (*a*) P. Changenet, P. Plaza, M. M. Martin, Y. H. Meyer and W. Rettig, *Chem. Phys*., 1997, **221**, 311–322; (*b*) N. A. Rozanel'skaya, A. I. Bokanov, B. M. Uzhinov and B. I. Stepanov, *J. Gen. Chem. USSR*, 1975, **45**, 277–280.

36 (*a*) M. Culcasi, Y. Berchadsky, G. Gronchi and P. Tordo, *J. Org. Chem*., 1991, **56**, 3537–3542; (*b*) J. F. Blount, D. Camp, R. D. Hart, P. C. Healy, B. W. Skelton and A. H. White, *Aust. J. Chem*., 1994, **47**, 1631–1639; (*c*) A. I. Bokanov, P. Yu. Ivanov, N. A. Rozanel'skaya and B. I. Stepanov, *Russ. J. Gen. Chem*., 1975, **47**, 702–705.

37 (*a*) P. S. Pregosin and R. Kunz, *NMR: Basic Principles and Progress*, 1979, **16**, 47–55; (*b*) M. J. T. Ditty and W. P. Power, *Can. J. Chem*., 1999, **77**, 1951–1961, and references therein.

38 A. D. Bain, *Prog. Nucl. Magn. Reson. Spectrosc*., 2003, **43**, 63–103.

39 A. D. Bain and P. Hazendonk, *J. Phys. Chem. A*, 1997, **101**, 7182–7188.

40 F. H. Allen, O. Kennard, D. G. Watson, L. Brammer, A. G. Orpen and R. Taylor, *J. Chem. Soc., Perkin Trans. 2*, 1987, S1–S19.

41 A. J. Bard and L. R. Faulkner, *Electrochemical Methods: Fundamentals and Applications*, Wiley, New York, 2nd edn, 2001.

42 C. M. A. Brett and M. O. Brett, *Electrochemistry: Principles, Methods and Applications*, OUP, Oxford, 1993, p. 29.

43 Cited as 0.38 cP at 25 °C, in *Handbook of Organic Solvent Properties*, ed. I. M. Smallwood, Wiley, NY, 1996.

44 B. Merzougui, Y. Berchadsky, P. Tordo and G. Gronchi, *Electrochim. Acta*, 1997, **42**, 2445–2453.

45 M. Matsumoto and T. W. Swaddle, *Inorg. Chem*., 2004, **43**, 2724–2735.

46 $[Cc]^{+/0}$ −1.35 ± 0.01 V *vs.* $Fc^{+/0}$: R. S. Stojanovic and A. M. Bond, *Anal. Chem*., 1993, **65**, 56–64.

47 A. M. Bond, *Broadening Electrochemical Horizons. Principles and Illustration of Voltammetric and Related Techniques*, Oxford University Press, Oxford, 2002.

48 (*a*) Z. B. Alfassi, P. Neta and B. Beaver, *J. Phys. Chem. A*, 1997, **101**, 2153–2159; (*b*) P. K. Wong and A. O. Allen, *J. Phys. Chem*., 1970, **74**, 774–778; (*c*) H. D. Burrows, D. Greatorex and T. J. Kemp, *J. Phys. Chem*., 1972, **76**, 20–26.

49 M. Nakamura, M. Miki and T. Majima, *J. Chem. Soc., Perkin Trans. 2*, 2000, 1447–1452.

50 (*a*) M. Oyama, T. Higuchi and S. Okazaki, *Electrochem. Solid-State Lett*., 2002, **5**, E1–E3; (*b*) R. A. Kipp, J. A. Simon, M. Beggs, H. E. Ensley and R. H. Schmehl, *J. Phys. Chem. A*, 1998, **102**, 5659–5664; (*c*) T. Sumiyoshi, *Chem. Lett*., 1995, 645–6.

51 (*a*) M. P. Ferroud-Plattet, Y. Ayant, E. Belorizky and P. Tordo, *Solid State Commun*., 1991, **80**, 947–949; (*b*) C. Palau, Y. Berchadsky, F. Chalier, J.-P. Finet, G. Gronchi and P. Tordo, *J. Phys. Chem*., 1995, **99**, 158–163.

52 WinSim (v.0.98, 2002) software: D. R. Duling, *J. Magn. Reson. B*., 1994, **104**, 105–110.

53 The relative sizes of the isotropic ^1H–^{31}P coupling constants of the neutral phosphine were used as a guide for these simulations. Note that the values obtained in simulation are in excellent agreement with the calculated hfc values for these two H atom sites, so long as dynamic averaging of the static structure is allowed for in the solution values (average of H4 and H6 = 0.16 mT; of H7 and H10 = 0.10 mT)—see Table S3, ESI†.

54 (*a*) A. V. Il'yasov, Yu. M. Kargin, E. V. Nikitin, A. A. Vafina, G. V. Romanov, O. V. Parakin, A. A. Kazakova and A. N. Pudovik, *Phosphorus Sulfur*, 1980, **8**, 259–262; (*b*) A. V. Il'yasov, Yu. M. Kargin and A. A. Vafina, *Russ. J. Gen. Chem*., 1993, **63**, 1833–1840.

55 N. G. Connelly and W. E. Geiger, *Chem. Rev*., 1996, **96**, 877–910.

56 L. Song and W. C. Trogler, *Angew. Chem., Int. Ed. Engl*., 1992, **31**, 770–772. The review by Connelly and Geiger lists the potential of the $Ag^{0/+}$ couple in CH_3CN solution as only +0.04 V *vs.* $Fc^{+/0}$. Consistent with this value, we found that $AgClO_4$ in CH_3CN is incapable of generating the $Dipp_3P^{+\bullet}$ radical.

57 (*a*) J. F. Blount, C. A. Maryanoff and K. Mislow, *Tetrahedron Lett*., 1975, 913–916; (*b*) P. Finocchiaro, D. Gust and K. Mislow, *J. Am. Chem. Soc*., 1974, **96**, 2165–2167; (*c*) J. D. Andose and K. Mislow, *J. Am. Chem. Soc*., 1974, **96**, 2168–2176; (*d*) K. Mislow, *Acc. Chem. Res*., 1976, **9**, 26–33.

58 N. N. Greenwood and A. Earnshaw, *Chemistry of the Elements*, Butterworth-Heinemann, Oxford, 2nd edn, 1997, p. 493.

59 (*a*) D. G. Gilheany, *Chem. Rev*., 1994, **94**, 1339–1374; (*b*) T. A. Albright, J. K. Burdett and M.-H. Whangbo, *Orbital Interactions in Chemistry*, Wiley, New York, 1985.

60 It is well-known that longer E–Si bonds allow for much lower barriers to pyramidal inversion, and that the ground state structures of trisilylamines are often planar.[59] By contrast, $P(SiR_3)_3$ usually retain pyramidal ground state structures. For example, in $Mes^*P(SiMe_3)_2$, $\sum\angle$(C, SiPC, Si) = 343.2(1)° (*a*) A. H. Cowley, M. Pakulski and N. C. Norman, *Polyhedron*, 1987, **6**, 915–919. In $P(SiMe_3)_3$, $\sum\angle$(SiPSi) = 318.07°; (*b*) J. Bruckmann and C. Kruger, *Acta Crystallogr., Sect. C*, 1995, **51**, 1152–1155. However, in the more congested $P(Si^iPr)_3$, $\sum\angle$(SiPSi) = 359.789(3)°;

(*c*) M. Driess, K. Merz and C. Monse, *Z. Anorg. Allg. Chem.*, 2000, **626**, 2264–2268; (*d*) C. von Hänisch, *Z. Anorg. Allg. Chem.*, 2001, **627**, 1414–1416. The implication of these results is that P–Si conjugation significantly lowers the barrier to pyramidal inversion compared to P–C bonds, but that the effect is smaller than for N; though pyramidal remains the preferred geometry, steric effects compete effectively.
61 G. H. Penner and R. E. Wasylishen, *Can. J. Chem.*, 1989, **67**, 1909–1913.
62 C. A. Jolly, F. Chan and D. S. Marynick, *Chem. Phys. Lett.*, 1990, **174**, 320–324.
63 A. Rieker and H. Kessler, *Tetrahedron Lett.*, 1969, 1227–1230.
64 (*a*) B. I. Stepanov, V. M. Matyuk, A. I. Bokanov and E. N. Karpova, *J. Gen. Chem. USSR*, 1975, **45**, 2059–2060; (*b*) V. V. Negrebetskii, A. I. Bokanov, L. Ya. Bogel'fer, N. A. Rozanel'skaya and B. I. Stepanov, *J. Gen. Chem. USSR*, 1978, **48**, 1196–1197; (*c*) V. V. Negrebetskii, A. I. Bokanov, N. A. Rozanel'skaya and B. I. Stepanov, *J. Gen. Chem. USSR*, 1979, **49**, 1304–1306; (*d*) V. V. Negrebetskii, A. I. Bokanov, L. Ya. Bogel'fer, N. A. Rozanel'skaya and B. I. Stepanov, *J. Gen. Chem. USSR*, 1978, **48**, 1196–1200.
65 A. J. Bellamy, R. O. Gould and M. D. Walkinshaw, *J. Chem. Soc., Perkin Trans. 2*, 1981, 1099–1104.
66 H. E. Birkett, J. C. Cherryman, A. M. Chippendale, P. Hazendonk and R. K. Harris, *J. Mol. Struct.*, 2002, **602–603**, 59–70.
67 (*a*) A. S. Romakhin, E. V. Nikitin, O. V. Parakin, Yu. A. Ignat'ev, B. S. Mironov and Yu. M. Kargin, *J. Gen. Chem. USSR*, 1985, **56**, 2298–2301; (*b*) A. S. Romakhin, F. M. Palyutin, Yu. A. Ignat'ev, E. V. Nikitin and Yu. M. Kargin, *J. Gen. Chem. USSR*, 1987, **58**, 1723–1724; (*c*) A. S. Romakhin, V. A. Zagumennov, E. V. Nikitin and Yu. M. Kargin, *Russ. J. Gen. Chem.*, 1995, **65**, 1208–1212; (*d*) F. Chalier, Y. Berchadsky, J.-P. Finet, G. Gronchi, S. Marque and P. Tordo, *J. Phys. Chem.*, 1996, **100**, 4323–4330; (*e*) B. Merzougi, Y. Berchadsky, P. Tordo and G. Gronchi, *Electrochim. Acta*, 1997, **242**, 2445–2453.
68 G. Gritzner and J. Kuta, *Pure Appl. Chem.*, 1984, **56**, 461–466.
69 Interestingly, the contribution of methyl groups to the redox potentials of metallocenes have similar magnitudes: $Cp^*_2Fe^{+/0}$ is about 0.33 V more cathodic than $Fc^{+/0}$, equivalent to about 0.03 V per methyl group.
70 The "pyramidalization angle" is defined in refs. 36*a* and 51*b* as the angle by which the P–C bond is bent down from the horizontal (*i.e.* flat geometry.) This is not easily measured from modern software that relies on internal coordinates, or from compiled X-ray crystallographic data, for which the sums of angles around phosphorus $\sum\angle$(CPC) is much easier to obtain. Tordo's α can be obtained from such data using the following trigonometric relationship: $\alpha = \cos^{-1}[\sin\{\sum\angle(\mathrm{CPC})/6\}/\cos 30^\circ]$.
71 While it is tempting to apply similar reasoning in the comparison with unsubstituted Ph_3P and both Xyl_3P and Mes_3P, comparisons with fully irreversible and reversible redox couples must be discouraged; the effect of follow-up reactions on the potential of $Ph_3P^{0/+}$ are in fact likely to have shifted the apparent E° in the cathodic direction.
72 (*a*) G. Schiavon, S. Zercchin and G. Cogoni, *J. Electroanal. Chem.*, 1973, **48**, 425–431; (*b*) J. A. Caram and E. J. Vasini, *Electrochim. Acta*, 1994, **39**, 2395–2400; (*c*) P. Tordo, in *Landolt-Bornstein, New Series, Magnetic Properties of Free Radicals*, ed. H. Fischer, Springer, Berlin, 1988, Group 2, vol. 17e, Part 9, pp. 254–313.
73 V. A. Zagumennov and E. V. Nikitin, *Russ. J. Electrochem.*, 2003, **39**, 1236–1239.
74 S. Yamaguchi, S. Akiyama and K. Tamao, *J. Organomet. Chem.*, 2002, **646**, 277–281.
75 R. R. Schrock, M. Wesolek, A. H. Liu, K. C. Wallance and J. C. Dewan, *Inorg. Chem.*, 1988, **27**, 2050–2054.
76 An alternative route for the synthesis of $Dipp_3P$ is the reaction of purified $DippPCl_2$ with two equivalents of $(DippCu)_x$ in aliphatic hydrocarbons (*e.g.* refluxing *n*-heptane). We found that the yields from this procedure are considerably lower than that of the *in situ* procedure described here, despite the fact that the copper reagent has been structurally characterized and is prepared in pure form.[28] Solvent may play a role.
77 Bruker AXS Inc., Bruker SMART v 5.631, 2003.
78 ROTAX: Simon Parsons & Bob Gould, University of Edinburgh with additions by Richard Cooper (Oxford) and Louis Farrugia (Glasgow). Version 26th November, 2001.
79 G. M. Sheldrick, *SHELXTL. Version 6.14*, Bruker AXS Inc., Madison, WI, USA, 2003.
80 VNMR manual. Varian, Inc., USA, 2000.
81 A.D. Bain, 1995; based on the SIFFIT program described in: D. R. Muhandiram and R. E. D. McClung, *J. Magn. Reson.*, 1987, **71**, 187–192.
82 C. Cobas, J. Craces and J. Sandina, *MestRe-C 2.3a*, Dept. de Quimica Organica, Univ. de Santiago de Campostella, Spain, 1996–2000.
83 Mathworks, Inc., Matlab 6.5, 2002.
84 Hypercube, Inc., HyperChem Release 7.52 for Windows.
85 M. J. Frisch, G. W. Trucks, H. B. Schlegel, G. E. Scuseria, M. A. Robb, J. R. Cheeseman, V. G. Zakrzewski, J. A. Montgomery, Jr., R. E. Stratmann, J. C. Burant, S. Dapprich, J. M. Millam, A. D. Daniels, K. N. Kudin, M. C. Strain, O. Farkas, J. Tomasi, V. Barone, M. Cossi, R. Cammi, B. Mennucci, C. Pomelli, C. Adamo, S. Clifford, J. Ochterski, G. A. Petersson, P. Y. Ayala, Q. Cui, K. Morokuma, D. K. Malick, A. D. Rabuck, K. Raghavachari, J. B. Foresman, J. Cioslowski, J. V. Ortiz, A. G. Baboul, B. B. Stefanov, G. Liu, A. Liashenko, P. Piskorz, I. Komaromi, R. Gomperts, R. L. Martin, D. J. Fox, T. Keith, M. A. Al-Laham, C. Y. Peng, A. Nanayakkara, C. Gonzalez, M. Challacombe, P. M. W. Gill, B. G. Johnson, W. Chen, M. W. Wong, J. L. Andres, M. Head-Gordon, E. S. Replogle and J. A. Pople, *GAUSSIAN 98 (Revision A.9)*, Gaussian, Inc., Pittsburgh, PA, 1998.
86 *DigiSim for Windows 95*, Version 3.05; Bioanalytical Systems Inc., West Lafayette, IN, 2000.
87 A. Neudeck and L. Kress, *J. Electroanal. Chem.*, 1997, **437**, 141–156.
88 J. E. Wertz, P. Auzins and J. W. Orton, *Discuss. Faraday Soc.*, 1961, **31**, 140–150.
89 Bruker Analytische Messtechnik GmbH, *WINEPR SimFonia* version 1.25, 1996.